

A Multiscale and Multimethod Approach to Assess and Mitigate Concrete Damage Due to Alkali–Silica Reaction

Frank Weise,* Julia von Werder, Tanja Manninger, Bärbel Maier, Matthias Fladt, Sebastian Simon, André Gardei, Desirée Hoehnel, Stephan Pirskawetz, and Birgit Meng

Alkali–silica reaction (ASR) is a chemical reaction within concrete which can lead over time to cracking and spalling. Due to the complexity of the problem, it still causes damage to concrete constructions worldwide. The study aims to illustrate the interdisciplinary research of the German Federal Institute for Materials Research and Testing (BAM) within the last 20 years, considering all aspects of ASR topics from the macro- to the micro-level. First, methods for characterization and assessment of ASR risks and reaction products used at BAM are explained and classified in the international context. Subsequently, the added value of the research approach by combining different, preferably nondestructive, methods across all scales is explained using specific examples from a variety of research projects. Aspects covered range from the development of new test setups to assess aggregate reactivity, to analysis of microstructure and reaction products using microscopical, spectroscopical, and X-ray methods, to the development of a testing methodology for existing concrete pavements including in-depth analysis of the visual damage indicator and the deicing salt input using innovative testing techniques. Finally, research regarding a novel avoidance strategy that makes use of internal hydrophobization of the concrete mix is presented.

of hardened concrete on the mesoscale are grains of aggregate embedded in a micro–nanostructured matrix, as shown in **Figure 1**. A wide range of natural or synthetic stones can be used as coarse or fine aggregate. The binding matrix is usually formed by hydration reaction of a cement with water, modified with other mineral additions and further admixtures, each of them in hundreds or even thousands of possible variations.^[3,4]

A proper mix design supported by comprehensive standards and guidelines and implemented by skilled professionals makes it possible to produce concrete for all categories from normal to ultrahigh-performance applications. The constituents must be specifically selected to match the desired concrete properties to the expected requirements and conditions of use. In this manner, dedicated concretes can be designed with high resistance to recognized aggressive processes.^[5,6]

1. Introduction

1.1. Concrete


Concrete is an enormously versatile material which is widely used for civil buildings, industrial constructions, and infrastructure. It is outstandingly adaptable to different requirements because its properties can be adjusted flexibly through the selection of the specific components in the concrete design process.^[1,2] After pouring fresh concrete, the resulting constituents

1.2. Alkali–Silica Reaction

This study addresses resistance to the alkali–silica reaction (ASR), a damage mechanism capable of causing severe problems in concrete constructions if the mixture composition is not properly adjusted to the concrete's exposure to external factors—either due to unexpected changes in environment or due to quality problems originating from the selection of one of the composites.^[7–11] ASR takes place in concrete when certain preconditions occur in a critical combination. Explained very simply and schematically visualized in **Figure 2**, the three basic requirements for ASR are the simultaneous presence and interaction of sensitive silica phases in the aggregate, mobile alkalis (i.e., Na and K) in the pore solution which are always part of the cementitious matrix, and sufficient moisture.

Siliceous phases with known or potential sensitivity are mineral components contained in many types of aggregate. Factors influencing their ASR sensitivity include not only the quantity, but also their reactivity (mineralogical aspects such as amorphousness and crystallinity) and the probability of direct contact with the alkaline pore solution (geometrical and physical aspects such as pore structure, microcracks). Petrographic characterization is therefore an important tool for assessing the proneness of a specific aggregate type to ASR.

F. Weise, J. von Werder, T. Manninger, B. Maier, M. Fladt, S. Simon, A. Gardei, D. Hoehnel, S. Pirskawetz, B. Meng
Department Safety of Structures
Bundesanstalt für Materialforschung und -prüfung (BAM)
Unter den Eichen 87, 12205 Berlin, Germany
E-mail: frank.weise@bam.de

 The ORCID identification number(s) for the author(s) of this article can be found under <https://doi.org/10.1002/adem.202101346>.

© 2022 The Authors. Advanced Engineering Materials published by Wiley-VCH GmbH. This is an open access article under the terms of the Creative Commons Attribution License, which permits use, distribution and reproduction in any medium, provided the original work is properly cited.

DOI: 10.1002/adem.202101346



Figure 1. Typical concrete meso/microstructure: aggregate made of multicomponent river gravel, solidified by a cementitious binding matrix (mineral phases of micro- and nano-size, composed of relicts of the original binder and filler components and their multiphase reaction products resulting from their reaction with water).

Aggregate is the main concrete constituent, comprising about 80% by weight. Concrete aggregate from local sources is preferable for the simple reason that transport is a huge economic factor. The tremendous regional variations of natural rock or gravel petrography, depending on their genesis and geological history, result in big differences in national approaches to ASR prevention. National guidelines or standards are mainly driven by regional experience. This, together with the immense complexity of factors influencing the risk of damage, explains the lack of internationally harmonized standards and guidelines even after 80 years of research and experience on ASR.

Cement, additions, and admixtures usually must declare their Na and K content (mostly summarized as alkali equivalent, i.e., Na_2O equivalent). Some rock minerals are also known to release alkalis. Additionally, some conditions for concrete constructions, such as marine environments or exposure to deicing salts, are very critical because they provide a huge source of alkali combined with moisture supply.

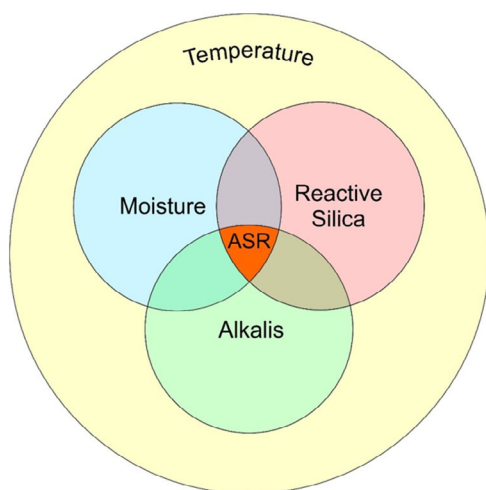


Figure 2. The three basic requirements for an ASR, all of them influenced by temperature.

ASR according to Figure 2 only takes place when all three pre-conditions are met at the same time. It is therefore only necessary to exclude one of the three conditions to ensure that the concrete is safe. This means that if the concrete is not expected either to have contact with water (i.e., internal elements) or if the critical limit of alkali availability is not exceeded (some standards and guidelines provide limiting values for cements), no ASR damage potential is to be expected, even if an ASR-sensitive aggregate is used. On the other hand, if neither moisture nor alkalis can be reliably excluded, great care is necessary to select an aggregate type that is insensitive to ASR.

Typical ASR damage patterns are shown in Figure 3. On the macro-level, characteristic netlike cracks give visual evidence of an accumulation of deformation and cracking on the micro-level, resulting from internal attack originating in aggregate grains. The primary cause is a reaction of the siliceous mineral phases with the alkalis, resulting in the formation of a gel-like, mainly amorphous reaction product (ASR gel). For very reactive aggregates, this reaction is easily identifiable under the microscope, as it is associated with intensive solution processes in the siliceous minerals of the aggregate and visible gel formation (see Figure 3b showing in its central area an aggregate grain identified as chert). But the involvement of ASR in a deterioration process is not always so obvious: natural aggregates occur in all intermediate stages from highly reactive to insensitive. In practice, the slow and late reaction of rocks with low sensitivity is a major problem. This type of ASR is more difficult to identify by testing and therefore sometimes appears unexpectedly several years after concrete production or construction. For example, Figure 3c shows a quartzitic grain with stressed quartz phases (a crystal deformation by metamorphosis). Here, a minimal reaction of the siliceous phase has already led to significant cracking because due to the minimal porosity of the rock, a very slight expansion is sufficient to provoke severe cracking.^[12] In general, both the reaction potential of the specific siliceous phase and the pore structure are the driving factors for the severity of the reaction.

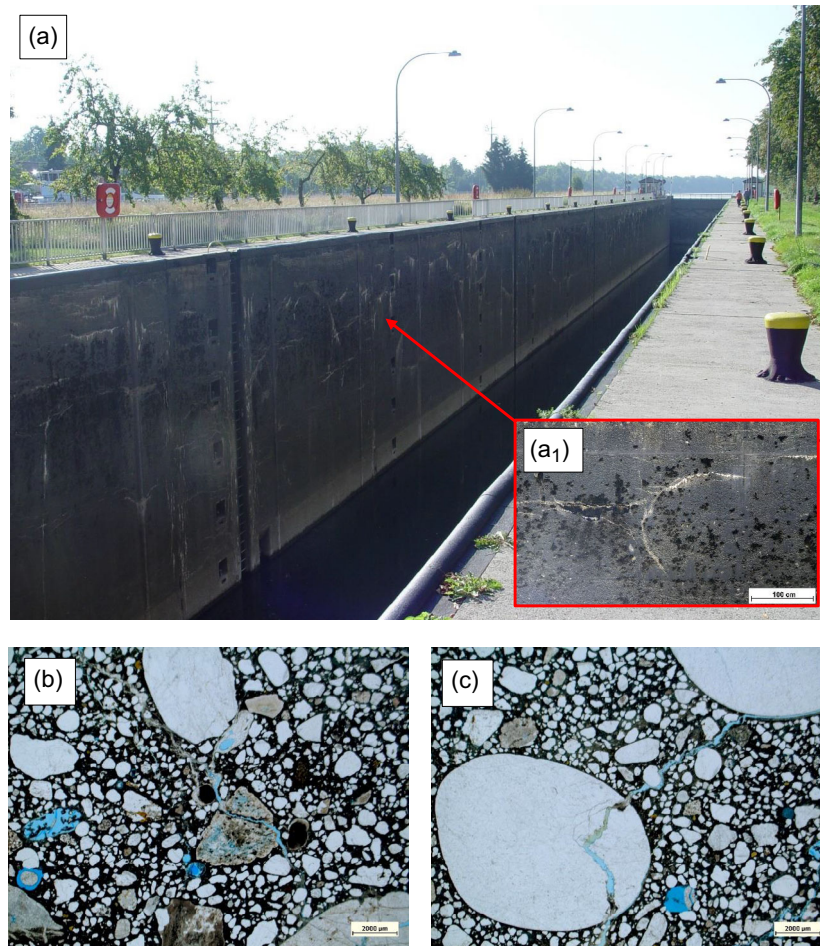


Figure 3. Double chamber lock Üfingen a) view of the lock wall with a₁) netlike cracks due to ASR of the aggregate as identified by microscopic analysis; b) siliceous aggregate with high reactivity: chert; c) siliceous aggregate with slow and late reaction: quartzitic rock.

1.3. Current State of Knowledge

Today's comprehensive state-of-the-art knowledge was achieved through experience with failed constructions built in the last 130 years,^[13–15] in particular by investigation of the reaction and failure mechanisms. ASR damage processes are comprehensively reflected in voluminous literature and in recommendations for concrete design.^[16–21] In particular, research has focused on criteria for the selection of constituents, while methodologies to assess the sensitivity or reactivity of aggregates play a key role.^[22] But despite 8 years of documented ASR research,^[23] knowledge is still evolving in exciting ways, leading to many new open questions to be tackled. This becomes evident through close scrutiny of conferences and studies dealing with many different aspects of ASR in the field and of basic materials science. The literature comprises: methodologies for classification of critical aggregate types, mitigation potential of the matrix composition, technologies for diagnosis and repair of damage, modeling of durability and remaining service life, etc. An unfailing source of knowledge is accumulated within the proceedings of the 15

International Conferences on Alkali-Aggregate Reaction in Concrete (ICAAR).^[24]

Currently, national approaches still address the locally available material resources and design concepts more precisely, but during the last 20 years great efforts have been made to evaluate the many and varied national experiences and to seek internationally accepted and more general approaches. International groups of scientific experts have taken an important role in stimulating and leading this process. Such communities organize themselves, for example, in the context of the International Union of Laboratories and Experts in Construction Materials, Systems and Structures (RILEM). Comprehensive documentation of the detailed consensus on ASR topics is available, based on the work of many RILEM Technical Committees (TC).^[8,25–30] These TCs address different facets of aggregate classification and damage evolution as well as further improving the international harmonization of appropriate testing procedures. Intensive interaction with the communities responsible for established standard testing procedures, for example, the American Society for Testing and Materials (ASTM International), is thus a matter

of course. RILEM expert groups have established a comprehensive petrographic atlas, employing microscopy techniques and proposing an international approach to provide a consistent procedure for the description and classification of rock types, including a uniform nomenclature.^[31] Other studies of these expert committees set the frame for categorizing and harmonizing accelerated ASR testing methods, including detailed explanations of the advantages and drawbacks of different strategies.^[8] Another important focus lies on the organization of round robin tests, and on the assemblage and overall evaluation of field tests^[32–35] which are an indispensable tool for the calibration of accelerated tests, including the definition of limit values with respect to measured expansions.

Organizations advancing construction codes such as the model codes issued by the International Federation for Structural Concrete (fib), and design codes published by the American Concrete Institute (ACI), have a great interest in incorporating internal attack associated with ASR into durability related performance criteria.^[36] Currently, however, due to the complexity of the subject matter, progress in integrating existing and emerging knowledge on proper material selection and durability testing parameters in structural design codes is slow.

One benefit of ongoing interaction with international research and prestandardization organizations (mainly RILEM) and standardizing committees such as ASTM (originally American Society for Testing and Materials) is that the established test procedures currently used, and new procedures emerging, follow more or less the same principles in most parts of the world.^[8,26,37–41] Harmonization is improving all the time with global interaction on the scientific level. An overview of the methodology currently used is provided in Section 3.

However, the situation appears to be more heterogeneous on the regulative level. Germany has a unique culture of preassessment and declaration for aggregate quality in relation to classes of ASR, which has the advantage of enabling straightforward action following the recommendations of the respective guideline (see Section 1.4). Other regions focus more on testing the real performance of a designed concrete mix, which makes it easier to consider potential alkali-binding potentials of the actual binder composition. Obviously, this provides more room for specific concrete design, but also has the big disadvantage of time delay because the accelerated testing procedures take several months.

1.4. Specific Situation in Germany

The ASR guideline issued by the German Committee for Reinforced Concrete (DAFStb) prescribes a procedure for classification, certification, and surveillance of aggregates according to their risk of inducing ASR in concrete.^[41] The test procedure comprises several stages and is based on a testing concrete so that independently of the specific application, the aggregate can be classified according to DIN EN 12 620: “aggregates for concrete”^[42] into an alkali-reactivity-class. The classification has the advantage that if the aggregates and applications are covered by the guideline they can be used immediately without further testing.

The ASR guideline further defines preventive measures for designing concrete mixes using aggregates of the different

classifications which depend on the humidity class of the application for the concrete specified in DIN 1045-2^[43] and in specific cases also on the cement content. The preventive measures range from the use of a cement with a low alkali content to replacement of the aggregate. For specific combinations of aggregate and humidity class, an expert report is also required. The guideline applies for all humidity classes (dry, humid, humid + external alkali supply) except for WS (impact of water, deicing salt, and heavy dynamic load, such as roads are subjected to).

Experience with applying the preclassification of available aggregate qualities in Germany according to the ASR guideline proved that ASR damage can be efficiently prevented in all but a few cases. There are exceptions, for example, in older constructions where adverse aggregates were used because their proneness to ASR was not yet known. Also, rather inhomogeneous river gravels, containing batches with a small proportion of a more sensitive material than expected, may be responsible for optical failures due to pop-outs close to single reactive grains (see Section 4.2). Furthermore, in particular cases, unclassified but sensitive aggregate was used, where it was not foreseen that the environment could provide alkalis (i.e., changes in exposure).

During the last two decades, major problems with ASR damage have mainly been reported for concrete pavements on highways. In Germany, these pavements are constructed without reinforcement and with sealed control joints. The concrete of the top layer is exposed to harsh stress by traffic (fatigue), thermal changes (dilatation in summer, frost), and moisture uptake (condensation, frost, deicing salts). Due to the combined exposure to such a multitude of physical, chemical, and mechanical loads, some aggregates which passed all guideline criteria to be classified as nonreactive were revealed to be problematic over time.

Some of these structures contained very slow and late reacting types of aggregate and the related damage could be clearly associated with ASR. Other damage at least indicated that ASR had contributed to the deterioration. The first examples of this type of damage in the early 2000s could be explained by the fact that the German alkali guideline at that time did not refer to these sensitive types of rock (i.e., graywacke from the eastern Elbe-Elster area and split gravel from the southern Rhine area^[44,45]). With the subsequent increase in experience of damage occurrence in practice, the German ASR guideline^[41] was gradually extended to cover these aggregate types. But some cases remained where the classification according to the guideline’s test methods failed to prevent damage. Clearly, the combination of loads revealed with respect to pavement concrete was so challenging that it was necessary to stipulate supplementary regulations. These additional rules, including expert opinions and intensified testing procedures,^[46,47] were authorized by the Federal Ministry of Transport and Digital Infrastructure (BMVI).

1.5. Motivation

The German Federal Institute for Materials and Testing BAM (Bundesanstalt für Materialforschung und -prüfung) is devoted to ensuring safety in technology and chemistry. In line with this mission, different research divisions with varying disciplines in BAM have been heavily involved with exploring ASR topics over the last 20 years. The range of activities covers research on many

ASR-related subjects, the elaboration of a wide variety of expert opinions and active participation in numerous national and international committees. Recent and current research has been focused on damage processes considering all aspects from the macro-level to the micro-level, also including basic parameters influencing reaction mechanisms and damage prevention.

The aim of this study is to illustrate and merge this interdisciplinary research by selection of exemplary methods, results, and approaches, including reference to the international state of knowledge.

Following the general introduction, Section 2 provides a description of analytical methods which are referred to in the subsequent sections.

Section 3 systematizes the most important approaches to accelerated laboratory tests for assessment of the ASR risk. The efforts within the international scientific community to harmonize these test principles, considering national characteristics, are briefly discussed. In this context, a study at BAM on a novel testing methodology for simultaneous tracking of internal microstructural changes during ASR concrete testing is presented.

Due to the central role of microstructure in ASR, Section 4 focuses on a few selected examples of material properties at the micro-level. The value added by combining different methods for physical and chemical microstructure analysis is exemplified by selected cases. Lastly, initial research results using Raman spectroscopy for the temporal and local characterization of amorphous reaction products are presented.

Finally, Section 5 gives an insight into BAM's ASR research activities on concrete pavements. An optimized test methodology for the condition and damage analysis of potentially ASR-damaged concrete pavements is presented as an example. In this context, innovative testing techniques for the determination of the cause of the initial damage indicator "darkening of the road surface" and for the analysis of deicing salt penetration are presented in more detail. Lastly, an insight into ongoing research on internal hydrophilization of concrete pavements as a novel ASR prevention strategy is provided.

2. Characterization Methods

Detailed analysis of the microscopic mechanism leading to the macroscopically observed phenomena of ASR damage is of vital interest because the initial formation of secondary phases due to the reaction is not visible on the macroscopic level. Optical microscopy and scanning electron microscopy (SEM) as well as Raman spectroscopy, 3D computer tomography (3D-CT), micro X-ray fluorescence analysis (micro-XRF), and laser-induced breakdown spectroscopy (LIBS) are utilized to accomplish this task.

Amorphous ASR gels filling cavities and cracks can easily reach sizes up to and over 100 μm while semicrystalline reaction products resulting from ASR are in the same dimension as cement hydrate phases, up to four orders of magnitude smaller. This means that the analytical methods used should not only be able to cover the microstructural level of object or phase detection, but the meso-level as well. The overall area investigated with a high local resolution needs to comprise a depth of several mm

or even cm, particularly if damage development is associated with depth-dependent structural changes. This is often the case when structural changes are concentrated closer to the exposed concrete surface or if intrusion processes, for example, of water bearing alkalis are involved. Such changes may correspond with gel formation, cracking, solution effects, or microchemical composition.

Additionally, in case of outdoor expositions associated with seawater or deicing salt application, the ingress of moisture as transport medium for alkalis into the concrete is a clear indication that problems due to ASR could arise.

Two nondestructive testing methods (NDT) are used for in situ moisture measurements on concrete components at BAM. Both radar and nuclear magnetic resonance (NMR) provide valuable data, complementary to each other on macro- and mesoscales.

To maximize information gain, different methods are often combined, as described in microstructural case studies in Section 4. This multimethod principle becomes even more valuable by extending it to combine these micro- and meso-level investigations with macroscopical approaches, as applied in the context of the research on concrete pavements explained in Section 5. The microstructural and analytical methods are referred to in Section 3–5. These methods were already mentioned above and are specified in the following subsections.

2.1. Microscopical Assessment

Optical microscopy is a standard tool used to gain insight into microcracking, identifying small-scale ASR precipitation and distinguishing it from other secondary reaction products (e.g., ettringite) in cracks and pores.

The technique is indispensable to confirm ASR and to evaluate the progress of deterioration. Thus, microscopic analysis is vital for damage analysis of existing structures, and for further evaluation related to specimens after accelerated testing. Petrographic determination of the aggregates, classification of their ASR sensitivity, and analysis of gel precipitation and crack patterns can help to further classify ASR damage.^[9,31]

The optical images shown in this study were acquired using a polarizing microscope (Zeiss Axioskop 40) or a stereo microscope (Olympus SZX16). Both devices use transmitted illumination in plane-polarized light (PPL) and cross-polarized light (XPL) and are equipped with a UV light source. The SEM image was acquired using the SEM Leo Gemini 1530 VP. The sample was covered with carbon to enhance the conductive properties.

The procedure for gaining information by microscopic analysis is briefly described in the following subsections. The explanations refer to a few exemplary pictures showing typical damage patterns including formation of ASR products (ASRP) and crack propagation for different types of aggregates.

2.1.1. Reactive Aggregates and Resulting Crack Patterns

Specific aggregates lead to various damage patterns, depending on the type and characteristics of the aggregate.^[48] The process of dissolution starts when grains containing the weakest silica parts come into contact with the alkaline pore solution.

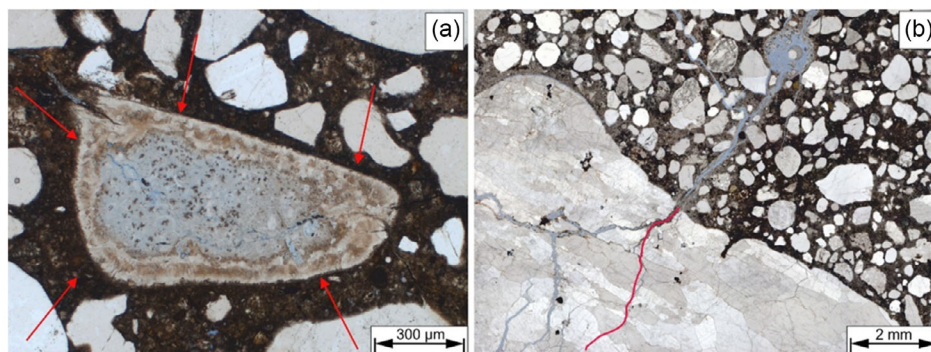


Figure 4. a) Grain with complete ASR rim (see arrows); b) ASR following intercrystal borders of distorted material (see line). Adapted with permission.^[50] published 2015; 15th Euroseminar on Microscopy Applied to Building Materials, Delft, The Netherlands.

The characteristic dissolution processes of highly crystalline aggregates composed mainly of silica are slow and confined in space close to the grain surface. Such aggregates can be classified as more or less inert.^[49] In contrast, aggregates containing amorphous and/or poorly crystalline forms of silica (e.g., opal or glass) are much more prone to dissolution in case of contact with dissolved alkali ions. The effect is enhanced if the aggregates are additionally characterized by a high porosity and thus provide more contact area. Polymineral aggregates (e.g., granite, graywacke, etc.) usually consist of pure silica (mainly quartz) with differing grades of crystallinity and other minerals (mainly feldspar and mica).

Cracks always originate from the aggregate. Their path, whether they pass through an aggregate grain, the hardened cement paste, or along the interface, is influenced by the mineralogy of the aggregate and by concrete technological factors so that the resulting damage symptoms can vary depending on the aggregate. The surface of microcrystalline quartz which dissolves completely is visible in the microscopic 2D picture as continuous reaction ring around the aggregate (**Figure 4a**). The distribution of cracks in gneiss follows the boundaries of the distorted quartz minerals in the grain (**Figure 4b**).

Cracks forming due to dissolution usually follow the most sensitive silica phases (lowest crystallinity). Fine-grained quartz aggregates like flint or chert show a uniform texture of interlocking grains. ASR damage manifests as individual linear cracks (**Figure 5a**). Aggregates comprising micro- or cryptocrystalline quartz varieties have an enhanced surface area and therefore a raised sensitivity to ASR. Silicious rocks can contain different sized and oriented quartz veins. However, if they do not contain

distorted silica phases, they do not contribute to the propagation of cracks from expansion through ASR (**Figure 5b**).

Pore volume accessible to the gel will delay or inhibit pressure build-up leading to crack formation.^[51] Connected pore volume can act as a transport area for moisture and alkali ingression while individual unconnected pores are beneficial to absorb the ASR gel formed.

2.1.2. ASRP

Cracks induced by ASR can be empty or filled either partly or completely with gel. The absence of gel, however, cannot exclude ASR as the cause of damage, on the one hand because the gel can be leached out by precipitation or sample preparation and on the other hand in the case of dense aggregate types with low reactivity. In the latter case, a typical ASR gel is not necessarily formed: even very little formation of (not gel-like) ASRP inside the rock can lead to severe cracking, due to the local lack of space for expansion.

Under PPL, amorphous silica gel appears mainly transparent. If a large amount of ASRP is formed (highly reactive aggregate), the gel often shows net-like cracks caused by shrinkage effects from drying (see **Figure 6**). These cracks form either during the service life of the concrete or due to sample preparation. Gel which progressed into cracks and air voids is often characterized by a mix of amorphous and crystalline parts. Under XPL the isotropic gel shows full extinction whereas the crystalline parts show only partial extinction or low birefringence.

The composition of the gel regarding the major oxides SiO_2 , CaO , Na_2O , and K_2O allows conclusions about its potential for

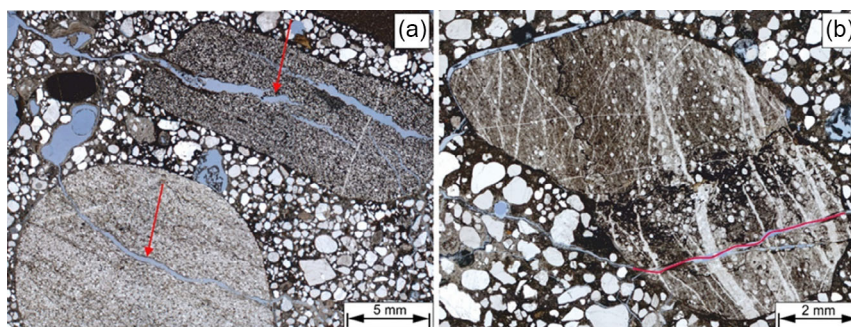


Figure 5. a) A grain of microcrystalline quartz with cracks through the grain matrix; b) siliceous rock with cracks straight through the grains. Adapted with permission.^[50]

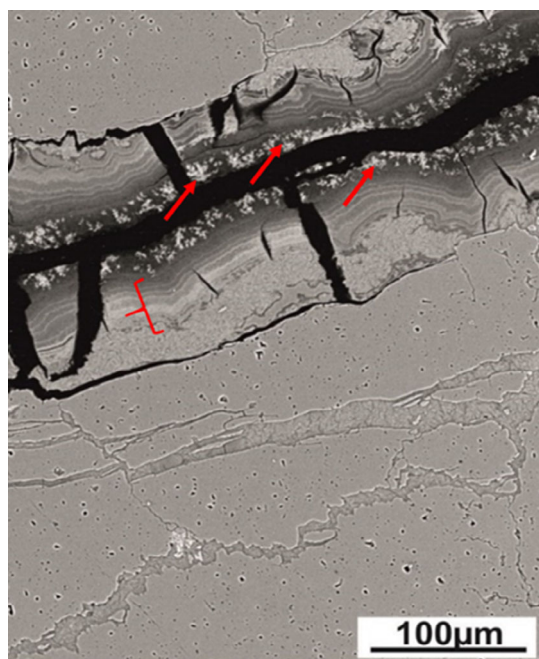


Figure 6. Back scattered electron (BSE) depiction of shrinkage cracks in ASR deposition. The gel shows signs of layers of multiple gel precipitation events due to wet dry cycles (see bracket). Parts of the gel show signs of crystallization (see arrows).

swelling^[52] (and subsequent crack formation) and can be analyzed chemically using SEM combined with energy-dispersive X-ray fluorescence analysis (EDX) or micro-XRF as described in Section 2.4. The process of subsequent gel formation over a longer time period can lead to layers of ASR gel as seen in Figure 6 which shows a zoning of different ASR product compositions within the crack filling. The lighter the gray level, the greater is the mass absorption coefficient of the elemental composition. In this case, the incorporation of K and Ca into the ASR products leads to higher mass absorption coefficient and therefore a lighter grey level.

As shown, microscopic analysis of enhanced thin sections and slides make it possible to assign deterioration mechanisms to specific areas of the concrete matrix, enabling researchers to choose suitable additional methods to deepen the understanding of the damage process.

2.2. Raman Spectroscopy

Raman spectroscopy is of special interest because of the general difficulty of characterizing ASRP, due to variability in the structures which are partly amorphous or of low crystallinity.^[53,54] The chemical composition and structure of ASRP differ greatly depending on the development conditions and change with the aging of the concrete.

Raman spectroscopy is known as a fast, versatile method for detecting smallest changes in amorphous and crystalline structures.^[55] It is especially suitable for the investigation of amorphous structures and also applicable for in situ measurements. The amorphous ASRP is usually present as gel-like phase.

Like silicate glasses, ASR gels are composed of a SiO_2 network where large cations (Na, K, Ca) act as network modifiers and induce the depolymerization of the network.^[55] To describe the degree of polymerization, the number of bridging oxygens (BO) in the SiO_2 network is indicated as Q species (Q^n), where “n” describes the number of bridging oxygens.^[56]

ASRP consists of layers of SiO_4 tetrahedra with three bridging oxygens (Q^3) and a smaller amount of SiO_4 tetrahedra present as chains with two bridging oxygens (Q^2) surrounded by channels and interlayer space. Both channels and interlayers permit the incorporation of Na, K, Ca, and H_2O .^[57–61] The chemical environment of ASRP formation and thus the inclusion of different ions into the gel structures is of huge interest in this line of work.^[62]

After identification of the ASRP products by means of polarized light microscopy, a Raman spectrometer LabRAM HR 800 (Horiba Scientific) equipped with a CCD detector and a BX41 microscope (Olympus) was used. The laser (Nd:YAG laser, $\lambda = 532 \text{ nm}$) is focused on the surface by a lens and has a spot diameter of about $1.5 \mu\text{m}$.^[63]

2.3. 3D-CT

3D-CT can be used to visualize and localize cracks and potentially ASR-damaged rock grains in drill cores. As it is a nondestructive technique, it is helpful in selecting interesting areas for the preparation of specialized thin sections, or checking the time-dependent development of deterioration during accelerated testing.

The measurement principle of 3D-CT (Figure 7) is based on the penetration of the sample with X-rays. While the sample is rotating around its own axis, the radiation enters the sample from different angles along its perimeter. This produces many individual images of the radiographic density distribution from which the geometric distribution of the absorption coefficients in the sample is calculated by means of special reconstruction algorithms (Figure 7). The locally different absorption of X-rays allows the concrete structure to be displayed and cracks to be clearly identified. For the analysis of drill cores with a diameter of 100 mm as described in Section 4.1, both a 3D microfocus installation with a 320 kV X-ray tube and an $\alpha\text{-Si}$ flat detector of 1024×1024 pixels were used. The setup results in a local resolution of radiographic density of about $100 \mu\text{m}$.

2.4. Micro-XRF

Micro-XRF enables the recording of elemental distribution mappings of sections or thin sections and is therefore a helpful tool to detect ASR gels by their increased sodium content and to identify depth-dependent processes related to ASR damage and of secondary ettringite formation, which often appears in combination with ASR. It is further used complementarily to support optical microscopy or Raman spectroscopy by identifying areas of interest for further research, based on their sodium content or Ca to Si ratio. Additionally, it is applied to differentiate between different aggregates and the cementitious matrix in cases where further interpretation is based on a quantitative separation of these components (segmentation by image analysis; an example similarly utilized for LIBS evaluation is described in the next subsection).

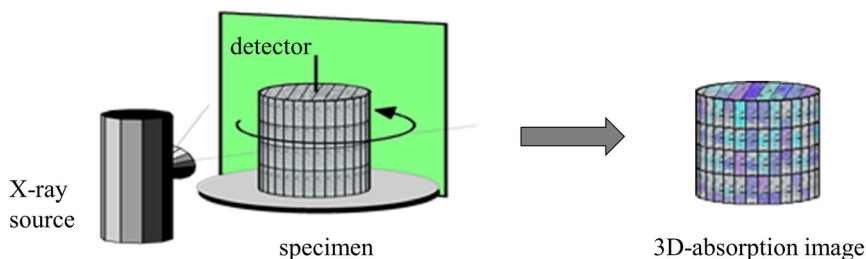


Figure 7. Measurement principle of 3D-CT.

The method is based on the X-ray fluorescence analysis of samples. The X-ray beam stimulates element-characteristic fluorescence by ionizing electrons from inner shells of the atom prompting outer shell electrons to take their places, leading to the emission of element-specific X-ray radiation. Fluorescence spectra of individual points or selected lines and areas (2D scan) are recorded by semiconductor detectors and analyzed. The method is only applicable for surface analysis with a penetration depth of 2–50 μm depending on the material.^[64]

The micro-XRF at BAM has a limit of detection (LoD) of 3 wt% for sodium and less for all other elements, depending on different measurement and sample conditions. The smallest possible diameter of the X-ray beam is 20 μm , therefore easily reaching the size range of ASR phases formed in cavities and cracks (over 100 μm) while regular cement hydrate phases are smaller by magnitudes and cannot always be distinguished.

2.5. LIBS

The use of LIBS was developed in view of the fact that a decisive element in promoting ASR damage processes may be the application of alkalis by winter services. Up to now, wet-chemical tests to determine the depth profile of sodium and chlorine in existing concrete pavements have only been carried out sporadically.^[65] This approach has the disadvantage that it is technically rather complex and delivers only limited spatial resolution. LIBS opens completely new possibilities for analyzing external deicing salt penetration in concrete pavements.

The LIBS measuring principle is shown in the diagram in **Figure 8a**. A pulsed, focused laser beam is applied to the surface of the building material. The high-power density of the laser

beam leads to vaporization of a small area, generating plasma of such high temperature that it breaks down all chemical compounds. In addition, the electrons in the individual atoms are brought to a higher energy level. During the subsequent expansion and cooling of the plasma, it emits first a continuous spectrum and then an element-specific line spectrum. The latter is only present if the electrons in the atom pass from an energy-rich to an energy-poor level (e.g., from ENiv. 2 to ENiv. 1 or ENiv. 0, or from ENiv. 1 to ENiv. 0). The different elements in the vaporized volume can be identified by spectroscopic analysis of the radiation wavelengths. In addition, the intensity of the radiation enables conclusions to be drawn about the concentration of individual elements. This makes it possible to quantify the elements by calibration with samples of defined composition. The measurements at BAM were carried out using the company SECOPTA analytics GmbH's FiberLIBS-lab-System (Figure 8b). For the automatic evaluation, BAM's own software tools were created in LabVIEW. Because the primary objective was to analyze the ingress of externally applied alkali into the cement paste, aggregates were excluded from the evaluation using a calcium threshold. More detailed information on LIBS applications for analyzing construction materials can be found in the literature.^[66–71]

2.6. Radar

Integral moisture measurement using radar is based on the increased permittivity of dry concrete after water ingress scaling from 4–6 to 8–14, depending on how much water is present in the pore space.^[72] This, in turn, reduces the diffusion speed of the electromagnetic waves in the test object, thus delaying reflection

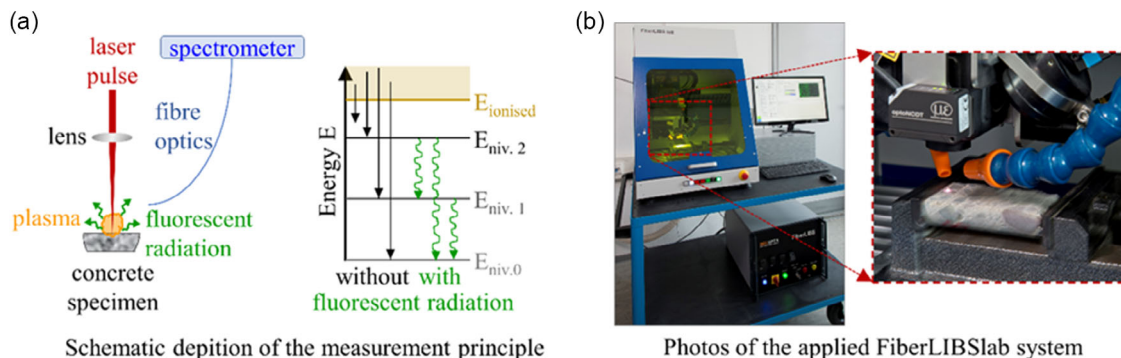


Figure 8. Description of the LIBS measurements. Adapted with permission.^[80] Copyright 2018, Ernst & Sohn.

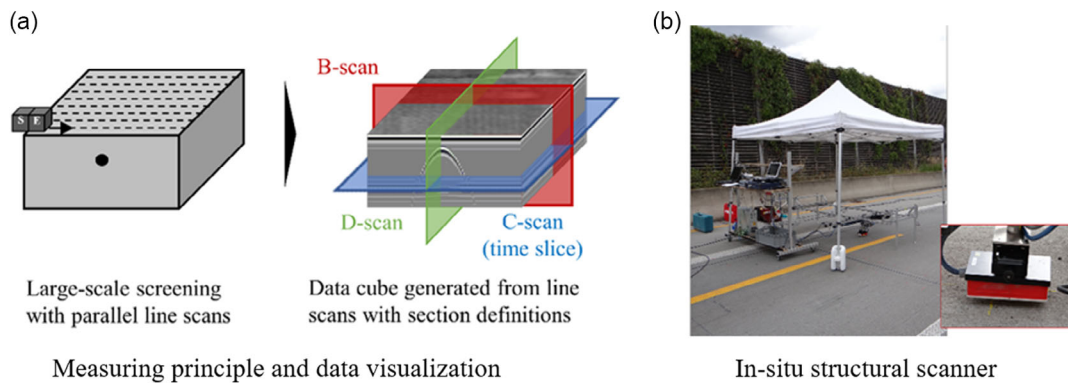


Figure 9. Description of the radar measurements: a) measuring principle and data visualization; b) in situ structural scanner. Adapted with permission.^[115] Copyright 2018, Ernst & Sohn.

of the signal from the back wall. For extensive, local high-resolution determination of lateral moisture distribution in the concrete pavement in Section 5.2, the measurement lines parallel to the transverse joint were 1 cm apart (Figure 9a). A data cube was generated from the radargram (B scan) gained from the individual measurement lines. From this data cube cuts were laid parallel to the concrete pavement surface and vertical to the B scans to generate C scans (time slices) and D scans. The measurements were made using a universal radar scanner with a 2.6 GHz ground coupled antenna. The structural scanner used for the fast, automated process with a pair of antennas on the concrete pavement slab was developed at the BAM (Figure 9b).

2.7. Nuclear Magnetic Resonance Relaxometry

High-resolution moisture measurement using NMR relaxometry is based on the interplay of hydrogen nuclei present in the concrete with a magnetic field introduced from outside and additional electromagnetic impulses. A higher NMR amplitude correlates with a greater moisture content. At BAM, the benchtop

measuring system of Magritek company's Mobile Universal Surface Explorer (MOUSE) PM 25 was used. With the specific measuring setup used, the sensitive volume is within the stray field of the primary magnets and reaches a depth of 120 μm . By placing the whole measuring apparatus vertically to the test object, the location of the sensitive volume can be varied from the test object surface up to a depth of 24.8 mm. Figure 10 shows how NMR relaxometry measurements on the highway pavement were carried out in practice.

3. Assessment of ASR Risk

Prevention of ASR damage is achieved by the application of different tests and the prescription of specific protective measures for concrete mixes based on the test results and the planned application of the tested aggregate. For existing structures showing typical signs of ASR deterioration, accelerated tests for assessing aggregate reactivity are applied to determine the residual damage potential. The current state of test methodology is described in the following sections.

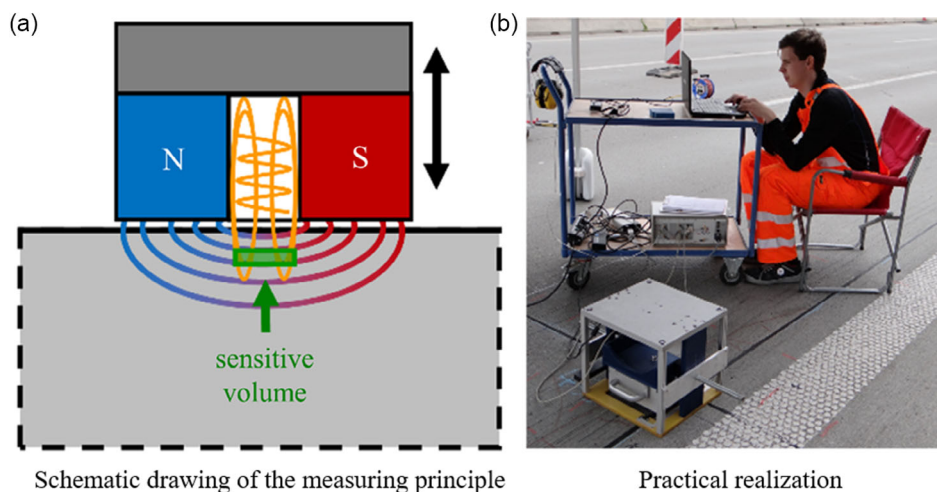


Figure 10. Description of the NMR-MOUSE (MOBILE Universal Surface Explorer): a) schematic drawing of the measuring principle; b) practical realization. Adapted with permission.^[115] Copyright 2018, Ernst & Sohn.

General tests for assessing aggregate reactivity can be divided into tests where the aggregate is assessed in isolation by petrographic and/or chemical analysis and those where aggregate performance is evaluated within a mortar or concrete matrix. Petrographic and chemical analysis provides fast results but does not allow any generalized projections regarding the aggregate tested. Its performance in the context of a cementitious matrix can only be assessed with mortar bar or concrete samples tests. Due to the slow kinetics of ASR (slow and late reactive aggregates), tests based on mortar or concrete samples must be accelerated.

In numerous studies, the results gained by applying different tests and standards to assess alkali reactivity of aggregates were compared and benchmarked against the behavior of structures in the field.^[17,32–35,73,74] Sources of reference for high-alkali cements and nonreactive aggregates were established for international and interlaboratory trials of accelerated tests. Contradictory results were carefully analyzed, and the methods have been continuously improved based on the resulting insights. Due to the long and intensive cooperation on European and international level as described in Section 1.3, the test procedures are now very similar in most parts of the world. In the following overview, ASTM standards and the internationally developed RILEM methods are therefore listed in addition to the national test methods as representative of the current state of knowledge.

3.1. Petrographic Analysis

Every aggregate assessment should ideally commence with petrographic analysis of the composition of the individual components to specify and quantify any potentially reactive constituents. Assignment of the aggregate to an alkali-reactivity-class (Table 1) together with other parameters makes it possible to determine further tests necessary to qualify and quantify aggregate reactivity. Also, after the application of accelerated tests, petrographic examination of the specimens is always recommended to confirm that any expansion was caused by a form of ASR.

Due to differences in detailed petrographic properties and qualities because of local geological history and petrogenesis, petrographers should apply local guidance and/or local experience to assist with this classification whenever possible. Under the third RILEM TC 219-ACS (alkali–aggregate reaction in concrete and structures), a worldwide petrographic atlas of reactive aggregates has been produced^[31] which is an essential adjunct to the RILEM Petrographic Examination Method AAR-1.1.^[26] The atlas contains a collection of micrographs of known and confirmed deleterious rock types and is intended to assist experienced

petrographers in the identification of potentially alkali-reactive rock types.

Sampling for the petrographic analysis is to be carried out in accordance with the national standards for sampling aggregates (EN 932-1, ASTM D75) and must be representative for the aggregates used in the concrete. The minimum mass to be received in the laboratory depends on the maximum particle size and ranges according to RILEM AAR-1 from 1 kg for aggregates up to 4 mm to 200 kg for a maximum particle size of 50 mm.

3.2. Chemical Analysis

Chemical test methods assess the alkali reactivity based on the behavior of the ground or crushed aggregates in basic, often heated, solutions. The criteria used for evaluation are the OH⁻ ion or the corresponding alkali concentration and/or the amount of dissolved silica in the solution as well as the mass loss of the aggregate. Research showed that solubility analysis is not universally applicable but depends on porosity as well as chemical and mineralogical compositions and crystalline structure effects. Due to the continuing debate, former standards such as ASTM C 289^[75] were withdrawn without replacement. In Germany, chemical analysis is part of the alkali guideline^[41] but is only used for the analysis of opaline sandstone and chert. To determine the mass loss after storage in sodium hydroxide solution, the minimum amount of opaline sandstone including chert and any questionable components depends again on the grade size and ranges from 400 g for grain fractions 1/2 to 7000 g for grain fractions >32 mm.

3.3. Accelerated Mortar Bar Test

Accelerated tests using mortar bars are an empirical approach, which relates the damage mechanism to the critical expansion of the samples due to the aggregate. They are based on a fixed mixture design in terms of testing cement, water-to-cement ratio, and tested aggregate.

To manufacture small scale mortar bars, coarse aggregates are crushed and screened, and the grain fractions combined according to a specified grading curve. Crushing and grinding of larger aggregates significantly enhances the reactive surface of the aggregate. Test requirements are further exacerbated by the particularly harsh storage conditions of the samples.

The accelerated mortar bar test described in the German alkali guideline is comparable to the NBRI method,^[37] the ASTM C1260-01,^[38] and the RILEM Test Method AAR-2,^[27] and comprises storage of samples manufactured in a defined way starting 1 day after manufacture until the age of 14 days in 80 °C hot NaOH solution. The dimensions of the mortar bars are either 40 × 40 × 160 mm [German alkali guideline] or 25 × 25 × 285 mm [ASTM]. The RILEM recommended test method AAR-2 comprises both mortar bar sizes (option AAR-2.1 and option AAR-2.2). The very strict testing conditions qualify aggregates as alkali sensitive which do not lead to damage in practice. The test procedure is therefore usually used only as a prescreening method which allows the quick identification of nonreactive aggregates. Test results showing that the aggregate

Table 1. Classification of aggregates.

RILEM	Alkali guideline (DAFStb)	
Class 1	E I	Very unlikely to be alkali-reactive
Class 2	E II	Potentially alkali-reactive or alkali-reactivity uncertain
Class 3	E III	Very likely to be alkali-reactive

is reactive need further analysis using the more representative accelerated concrete prism test.

3.4. Accelerated Concrete Prism Tests

The general procedure for accelerated concrete prism tests,^[8] for example, ASTM C1293^[39] and RILEM AAR-3,^[40] corresponds in many aspects to the accelerated mortar bar test. The main differences are that the aggregates are tested in the grain sizes that are used in practice, leading to bigger sample sizes of $75 \times 75 \times 285$ mm. Furthermore, the prisms are stored for a longer time in a humid atmosphere (bucket, fog chamber, stainless steel container). The aim of accelerated concrete prism tests is to simulate as closely as possible the long-term behavior in the field in as little time as required for getting reproducible results. To be representative, accelerated tests must depict the sequence and mechanisms of the individual reactions which constitute ASR. Further, the reaction products formed and their effect on the matrix must be as representative as possible. The practical relevance of accelerated tests can be only assessed by correlation with samples exposed in the field for many years or by analysis of damaged structures. To speed up chemical reactions, accelerated tests are based on the elevation of temperature and humidity and the supply of additional alkalis.

The provision of a high level of effective alkalis can be achieved either by using a cement manufactured from clinker naturally characterized by a high alkali level, by boosting the alkalis of the cement—for example, by adding potassium sulfate into the mixing water—or by exposing the samples to alkaline solution. Although known, the impact of the type of alkalis (Na, K) is usually ignored and NaOH or NaCl in specific cases is chosen to prepare the exposure solution. The concrete prism test at 40 °C in the fog chamber of the German alkali guideline^[41] is very similar to ASTM C 1293^[39] and RILEM Test Method AAR-3.^[27] The faster concrete prism test at 60 °C, which is listed as an alternative method in the alkali guideline,^[41] corresponds to RILEM Test Method AAR-4.1.^[27]

Early research further showed that some aggregates are characterized by a “pessimism” behavior,^[76,77] meaning that expansion of concrete samples is maximized at a certain level of reactive constituent in the aggregate and progressively reduced for both greater and lesser levels. In these cases, the total combination of coarse and fine aggregates must be tested for a reliable assessment. It is also known that specific aggregates are not reactive themselves but influence the reactivity of the concrete mix by releasing alkalis.^[78] The validation of a specific test procedure to quantify the alkalis released from aggregates (RILEM AAR-8^[79]) is currently topic of the recently established RILEM TC ASR (risk assessment of concrete mixture designs with alkali reactive (ASR) aggregates). The availability of water and alkalis as well as temperature also influences hygroscopic swelling, shrinkage, and creep, which must be taken into account when evaluating expansion. Further, sample geometry, alkali leaching humidity gradients and subsequent transport processes due to heating and cooling of specimens during accelerated tests were identified as having a significant impact on the test results.^[18] To counteract the falsification of results due to the test setup, various measures were developed, systematically tested, and

continuously improved. Leaching of alkalis can be prevented by different measures. In Japan, for example, samples are wrapped in a defined impregnated fiber fabric made of polypropylene and covered by a foil. At the BAM, an automated expansion monitoring has been realized, described in detail in the following Section 3.5.^[80–82]

3.5. Accelerated Concrete Prism Tests with Automated Damage Monitoring

3.5.1. Background

The motivation to design a new, automated benchtop reactor originated from a research project (IGF project 15248N)^[83] in which for the first time, three successive phases were identified in the course of the ASR in various accelerated concrete prism tests at 60 °C^[81,84,85] by combined continuous strain, acoustic emission, and ultrasonic measurements. As shown in **Figure 11**, in the first phase the ultrasonic velocity increases rapidly, indicating ongoing hydration and development of the elastic modulus of the young concrete. The onset and further development of cracking in the second phase of the test can be detected by increasing acoustic emission activity. Simultaneously, the microcracks are sources of elastic waves and registered as “hits” by ultrasonic transducers. As a result of damage to the structure by microcracking, the ultrasonic velocity decreases while the expansion of the specimens increases. In the third phase, decreasing acoustic emission activity and decelerating expansion

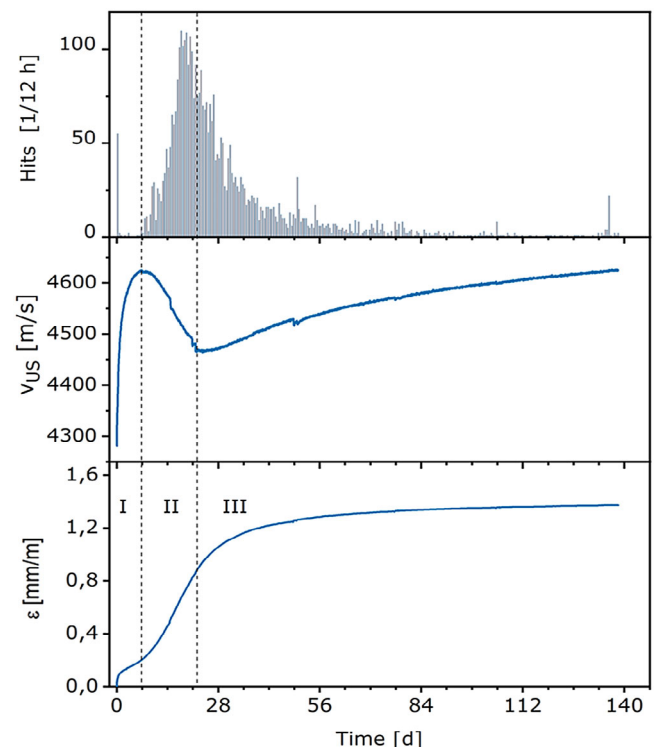


Figure 11. Three phases of ASR in the accelerated concrete prism test at 60 °C indicated by acoustic emissions, ultrasonic velocity, and expansion of the specimen. Reproduced under the terms of the CC BY.^[81]



Figure 12. Specimen (75 mm × 75 mm × 280 mm) in a measurement frame and the container (left), and benchtop reactor for six specimen containers (right). Adapted with permission.^[87] Copyright 2019, Ernst & Sohn.

indicate subsiding ASR. The increasing ultrasonic velocity in this phase can be explained by successive filling of the cracks with water and reaction products.

Based on successful damage monitoring, a compact and easy-to-handle system for automated ASR tests^[86] (Figure 12) was subsequently developed.

3.5.2. Features of the New Benchtop Reactor with Automated Strain Measurement

In collaboration with Schleibinger Testing Systems, a benchtop device was developed, where six specimens can be tested simultaneously, close to the accelerated concrete prisms tests at 60 °C described by RILEM Test Method AAR-4.1^[27] and the alternative method listed in the Alkali Guideline.^[41,86] Each specimen is installed in a measurement frame that is inserted above the liquid level into a container holding 3 cm of water.

Continuous recording of the specimen's expansion is realized by an eddy current sensor integrated in the top crosshead of the frame acoustic emission and ultrasonic velocity measurement technology can be installed as an option. Six of the containers can be stored in the benchtop reactor that ensures a constant temperature during the entire test and can be adjusted between 35 and 80 °C. A climate chamber such as that required for the monthly expansion measurement in the conventional test is not needed.

3.5.3. Comparison of Automated with Conventional Measurement

To validate the automated test system, the test results were compared to results obtained from conventional tests.^[87] The tested aggregates graywacke and quartz gravel can be identified clearly as alkali sensitive in both test setups as shown in Figure 13. The automated system detects the expansion limit being exceeded by

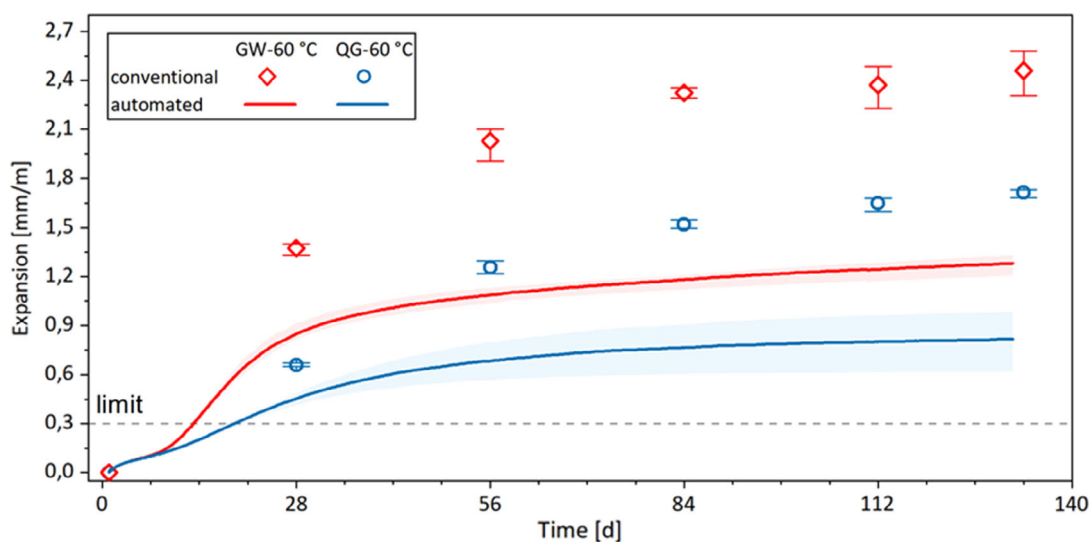


Figure 13. Accelerated concrete prism test at 60 °C: Expansions measured with a conventional test setup and with a prototype of the automatic benchtop reactor. Adapted with permission.^[87] Copyright 2019, Ernst & Sohn.

0.3 mm m⁻¹ as an indicator for high alkali reactivity according to Nixon and Sims^[88] after 13 and 18 days, respectively. Based on the data density, the test could be terminated a few days later. In addition, the data show that the ASR has nearly subsided after 56 days. In the conventional test, exceedance of the limit can only be detected after 28 days at the earliest. In case the expansion exceeds the limit only slightly, the test must be continued for at least 28 days.

The expansions measured are significantly smaller in the automated test compared to the conventional test. This can be attributed on the one hand to increased leaching of alkalis^[41] caused by a weakness of the design. As the top cover of the prototype container is slightly cooler than the container itself, water condenses on the top cover, drops on the specimen, and subsequently causes leaching. Heating for the top cover is integrated in the next generation of the device to avoid this unwanted effect. The second reason for the lower expansions measured with the new reactor is the constant temperature over the entire test period. Preliminary tests showed that cooling from 60 to 20 °C, as necessary in the conventional test, results in additional expansion.^[81] Cooling could be simulated in the automated test, but the results proved to be more stable and reliable when temperature changes are avoided. Therefore, it seems advantageous to determine a new, slightly lower limit for the automated setup in round robin tests rather than regular cooling of the specimen according to the conventional test.

3.5.4. Conclusion

The new device allows a high-resolution and continuous analysis of concrete prism expansion under accelerated testing conditions. In some cases, this allows earlier termination of the test. In general, the results are consistent with results of the conventional test even if the expansion measured by the automated test is systematically smaller. Supplementary tests are required to quantify the effect of intermediate cooling and to adjust the expansion limit for automated tests. Once installed, the test runs automatically, excluding human factors and an expensive climate chamber because the monthly manual expansion measurement is not needed. The benchtop reactor is also a valuable tool in the field of ASR research. The high resolution of expansion behavior allows detailed analysis of ASR kinetics and mechanisms, particularly in combination with acoustic measurement methods.

3.6. Performance Tests

In construction practice, aggregate mixtures are often used so that test results which classify individual aggregates are not applicable. Also, the use of supplementary cementitious materials and concrete technology parameters has an impact on the damage potential. To correctly include these factors, a concrete mixture designed for a specific application and moisture class can be tested. In this way it is sometimes possible to demonstrate the efficiency of concrete mixtures for which the alkali guideline specifies replacement of aggregate or use of (Na) cements, and to prevent the exclusion of regionally available aggregates or cements. For specific applications characterized by very tough environmental conditions, for example, road construction,

corresponding performance tests including alternating temperature loads and external alkali supply are mandatory in some countries.

Besides the assessment of a job mixture, performance testing can also be used to develop non-ASR-susceptible concrete mix designs for a regional worst-case scenario aggregate combination. The minimum amount of SCMs required for the use of the aggregate source or fraction at a defined maximum alkali level, or alternatively the alkali threshold with CEM I, can be determined by applying a systematic experimental design.

The same procedures are used for the performance tests as for concrete prism tests. RILEM AAR-10^[30] describes the concrete prism test at 40 °C in analogy to AAR-3.^[40] AAR-11^[30] offers the same concept but testing at 60 °C and therefore corresponds to AAR-4.1.^[27] To avoid leaching of alkalis and thus to ensure the ASR damage potential is accurately reflected during the various types of concrete prism tests, a procedure for wrapping concrete prisms is described in AAR-13.^[87] The wrapping consists of a defined carrier material impregnated with NaOH solution and an outer foil protecting the test specimen from drying out.

AAR-12^[86] describes a newly international introduced modified 60 °C prism test that has been used in Germany for more than 15 years is described. It includes a procedure for simulating a cyclic external alkali supply to evaluate aggregates and concrete compositions for concrete pavements on highways and airfields. As an alternative to this test method, cyclic climate storage testing is also used in Germany. The basic procedure for evaluating the alkali sensitivity of coarse aggregates for concrete pavements in Germany and a brief description of both prism tests with alkali supply can be found in Section 3.8.

3.7. Tests to Assess the (Residual) Damage Potential of an Existing Structure

For existing structures showing deterioration which could be caused by ASR, methods were developed to assess damage progress and residual damage potential. Differentiating between ASR and other damage mechanisms causing internal expansion like secondary ettringite formation, frost damage, or internal sulfate attack, and distinguishing whether the reaction is the primary or a contributory cause of the damage, are tasks for a particularly knowledgeable and experienced expert. Further, there is no standard method which can be used to select representative samples and drill cores for further laboratory analysis.

The German Committee for Reinforced Concrete^[41] has therefore only issued recommendations for damage diagnosis and repair of concrete structures affected by ASR. The combination of methods appropriate for the assessment of a specific structure must be selected by the appointed expert. The following procedures listed in the recommendations serve only as support and not as instructions to be blindly followed: 1) Analysis of all important preliminary information about the damaged building (inventory plans, construction diary, climatic conditions, concrete composition, concreting technology). 2) Visual assessment of the structure (aggregates, type, distribution, depth and width of cracks, efflorescence, and gel excretions). 3) Removal of drill cores for strength tests and regular assessment of residual expansion and increase in mass during storage in the fog chamber or

alternatively in a test setup with external alkali supply. 4) Nondestructive determination of the dynamic modulus of elasticity by measuring the ultrasonic time of flight, by natural frequency measurements, or by natural oscillation time measurement after impulse excitation. 5) Microscopic examination and petrographic characterization of aggregates based on polished cores and thin sections.

The abovementioned methods are reflected and further elaborated in the RILEM Recommended Test Methods AAR-6.1: Reliable diagnosis of damage from alkali reactions^[19] and RILEM AAR-6.2:^[20] Guidance for structures affected by AAR. While AAR-6.1 is devoted to diagnosis and describes the procedures for detecting damage caused by ASR, the objective of AAR-6.2 is to provide information and tools for assessing the performance of structures in terms of structural capacity, serviceability, and durability. It further includes a strategy for asset management based on a risk analysis defining the vulnerability and the criticality of the structure.

3.8. Procedure for the Prevention of ASR Damage in the Construction of New Concrete Pavements

As mentioned in Section 1.4 and 3.6, Germany follows a special path for avoiding the use of alkali-sensitive aggregates in concrete pavements. The use of aggregates is regulated by the General Circular on Road Construction (ARS) 04/2013.^[47] This applies to both new construction and complete replacement of concrete pavement on highways using load class Bk 100 to Bk 1.8 concrete (moisture class WS: subject to water, external alkali supply, and heavy dynamic load) in accordance with RStO 12 guidelines on standardizing road pavements.^[89] One of the three methods shown in **Figure 14** can be used to prove that the selected coarse aggregate in accordance with DIN EN 12620^[42] with grain reference sizes $d \geq 2$ mm, or the concrete pavement itself, is not prone to ASR. All three test procedures must be carried out by a recognized ASR expert appointed by the BAST in close collaboration with the BAM.

The V1 procedure proves the suitability of a particular concrete mixture in relation to avoiding damaging ASR for a specific construction project (performance test). If proof of the suitability of a coarse aggregate of grain size $d \geq 2$ from a particular deposit is

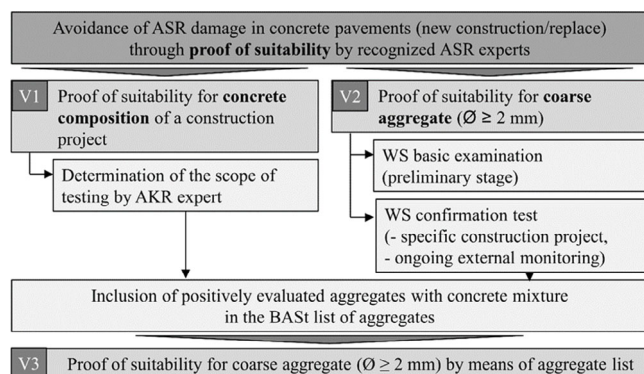


Figure 14. Possible procedures for suitability verification by recognized ASR experts to prevent ASR damage to concrete pavements following ref. [47].

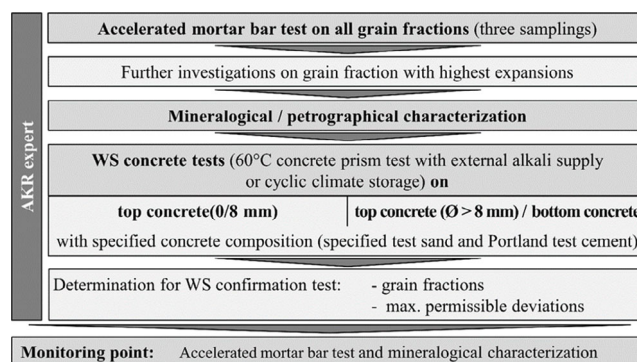


Figure 15. Test procedure for WS basic test according to V2 procedure based on ref. [47].

required to indicate that it is not ASR prone, independent of a specific construction project, the V2 procedure is applied, including the WS basic and confirmation tests. The test process can be seen in **Figure 15**.

For the basic WS test, all aggregates from a particular deposit intended for highway pavement construction are subjected to an accelerated mortar bar test. Based on the findings, the grain groups with the greatest expansion are subject to mineralogical/petrographic analysis. Next, the suitability of these grain groups is examined using a WS concrete test according to a prescribed concrete composition with specified test cement and test sand, taking the construction method into account. This can be carried out using a 60 °C concrete prism test with alkali supply^[86,90] or cyclic climate storage test.^[90] If the aggregate passes the WS basic test, a WS confirmation test must be carried out at defined time intervals or in good time before the concrete is used in the construction. The confirmation test includes both a repeat rapid test and mineralogical/petrographic analysis of all grain sizes of the coarse aggregate. Concrete compositions and aggregates that are positively evaluated by V1 and V2 methods are included in BAST's aggregate list and are the basis for suitability tests for coarse aggregates in accordance with V3 by a recognized ASR expert (Figure 14).

The 60 °C concrete prism test with alkali supply has been used in Germany since approximately 2005 to evaluate alkali-sensitive aggregates for concrete pavements.^[91] It is described in detail in the TP B-StB 1218a test procedure^[90] in AAR 12.^[30] In this test procedure, six test specimens are preconditioned in a defined way and subjected to a reference measurement, and then subjected to ten climate storage cycles (**Figure 16**). Each cycle comprises a 5-day drying phase at a temperature of $(60 \pm 2)^\circ\text{C}$, a 2-day immersion phase in the test solution (three test blocks each in a 10% and a 3% NaCl solution) at a temperature of $(20 \pm 2)^\circ\text{C}$, a 6-day storage phase out of water at a temperature of $(60 \pm 2)^\circ\text{C}$ (relative humidity at least 98%), and a 1-day cooling phase at a temperature of $(20 \pm 2)^\circ\text{C}$ (Figure 16). After this, the test blocks are removed for a maximum of 2 min from the closed stainless-steel containers to determine their length and mass. Linear expansion is taken as the primary ASR damage indicator. Its threshold value after ten storage cycles under changing conditions is 0.5 mm m^{-1} when using a 10% NaCl solution and 0.3 mm m^{-1} when using a 3% NaCl solution.

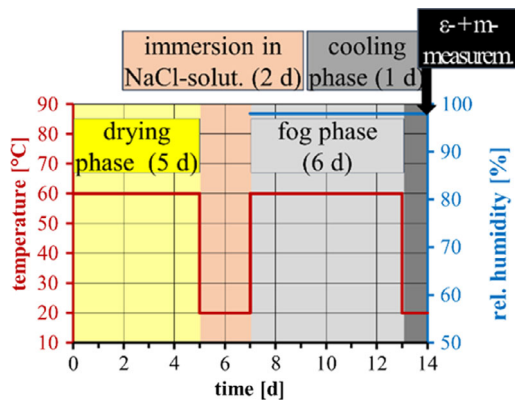


Figure 16. Storage regime in an alternating cycle in the 60 °C concrete prism test with alkali supply.

As an alternative to the 60 °C concrete prism test with alkali supply, cyclic climate storage test has also been used in Germany since about 2005.^[92] This test method has so far only been used at national level and is described in detail in a technical test regulation (TP B-StB 2018b).^[90] Six samples are subjected to 12 cycles of climate change storage. Each cycle consists of three phases: 4 days drying, 14 days fog storage, and a 3 day freeze-thaw-cycle phase (**Figure 17**).

The drying phase starts with heat shock exposure. After the drying phase at 60 °C and the subsequent cooling to 20 °C, a 3.6% NaCl test solution is applied to three specimens of each test series while demineralized water is applied to an additional set of three specimens for comparison. These test solutions remain on the specimens during the fog and freeze-thaw-cycle phases. After the freeze-thaw-cycle phase, the test solution is removed from the specimens and their mass and linear expansion changes are determined. The reference values for evaluating the changes to these values are determined in the first cycle after the drying phase. In the individual cycles, after the freeze-thaw-cycle phase, the test solutions for measuring the mass and linear

expansion of the test specimens are removed and then reapplied. After the drying phase, a new test solution is applied to the test specimens in each case.

The assessment criterion for ASR damage potential after cyclic climatic storage test is, again, linear expansion. The threshold value for laboratory concrete, depending on the test solution applied, is 0.4 mm m⁻¹ (water) and 0.5 mm m⁻¹ (NaCl solution). The increase in expansion between the sixth and eighth climatic storage cycles is also included in the assessment.

4. Microstructural Investigations—Multimethod Applications

This section provides a few case studies where a combination of different methods on the microscale was used to elaborate basic information. The background and aim for such studies may be very different for each specific case, but the questions to be addressed when ASR is considered to have a potential contribution to deterioration of concrete are usually the same. Therefore, the chosen examples provide some general aspects which are typical for the approach to research on damage mechanisms as well as expert reports or recommendations about prevention, prognosis, or repair of damage.

An assessment of the potential contribution of ASR as partial or main driving force for concrete damage always needs to consider the three main factors as outlined in Figure 2: sensitivity of the aggregate, and sources of moisture and alkalis. The combined measurement of the related microstructural and microchemical properties is a very effective and indispensable tool for such elaborations. But the reliability of the outcome is strongly dependent on appropriate preparative work. Caution is advised within all steps, starting with the sampling method (mostly drilling cores) and sample preparation for further analysis (cutting, drying, impregnation, grinding, polishing, etc.). The measuring conditions also have decisive impact on the representativity of the results.

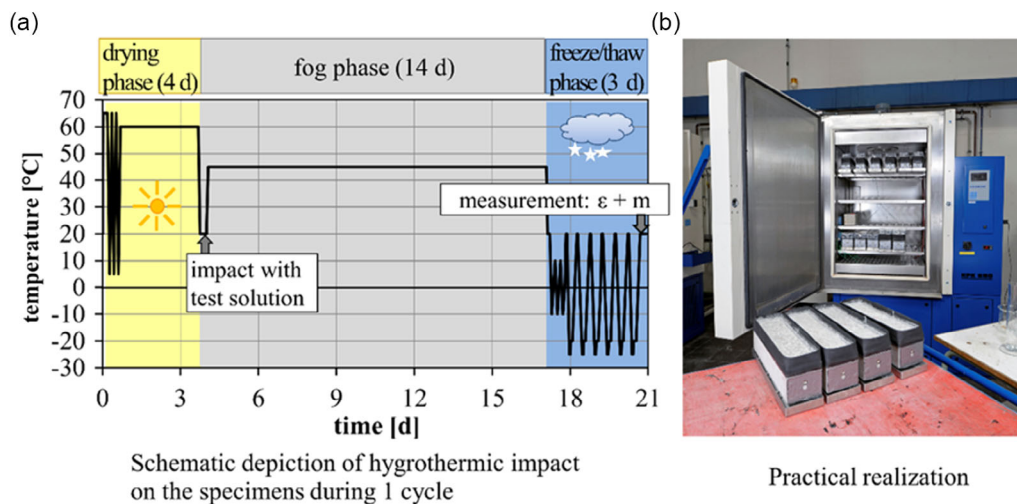


Figure 17. Description of cyclic climatic storage test. Schematic depiction of hygrothermic impact on the specimens during one cycle. b) Practical realization.

The first two case studies were selected to illustrate the complementary evaluation of different microscopical techniques, micro-XRF and 3D-CT. Finally, we present a recent and still ongoing study on utilization of Raman spectroscopy for further characterization of the amorphous or semicrystalline gel substances.

4.1. Innovative ASR Damage Analysis on a Hydraulic Structure

The double chamber lock in Üfingen was already used as an example in Section 1.2. BAM was involved in the damage assessment during preparation of the repair of this structure. A combined testing methodology for both the structural and laboratory investigations was developed within this context.^[93] After the usual visual assessment, the interior of the lock wall was additionally examined for the first time with radar and ultrasound in reflection mode over a large area of two representative blocks of the chamber wall. Previously, it was only possible to obtain information about the internal structure at selected locations of the lock wall by sampling drill cores. The NDT findings indicated more severe and deeper structural damage (structural loosening, cracking, shell separation) in the water exchange zone. Visual signs of deterioration in form of net-shaped cracks with white efflorescence and spalling were also most prominent in this area. For calibration and validation of the findings of the nondestructive testing and determination of the cause of damage

in the laboratory, drill cores were taken from specially selected sampling points on the chamber walls of both blocks. For this purpose, a novel testing methodology consisting of 3D-CT, microscopy, and micro-XRF was used in the laboratory (Figure 18).

As a first step 3D-CT, described in more detail in Section 2.3, was applied to verify the microstructural changes recognized by NDT and to select regions for subsequent microscopic and microchemical investigation. Large-format thin sections (100 mm × 75 mm) were then prepared from this area for further investigations using a polarizing microscope, a scanning electron microscope with an energy-dispersive detector (REM-EDX), and the micro-XRF (see Section 2.4).

The virtual cross sections acquired by 3D-CT enable a 3D understanding of the crack pattern (Figure 19). In the gray-scale images, aggregates characterized by high radiographic density appear bright whereas cracks and pores stand out as dark due to their low radiographic density. The cementitious matrix exhibits its interim values. All images show a distinct crack formation, indicating combined structural damage caused by freeze-thaw stress and ASR. A crack pattern typical for ASR can be seen in the tagged area of Figure 19b where cracks originate from a severely damaged aggregate grain.

Further analysis of the aggregate grain by light microscopy and micro-XRF after preparation of a thin section identified the grain as a heavily decomposed silicious schist with

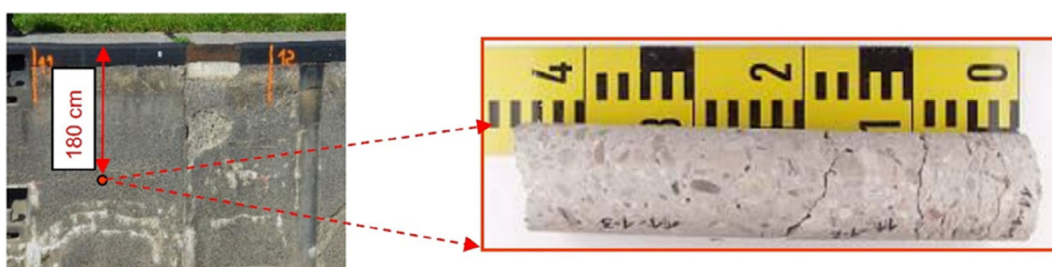


Figure 18. Place of extraction and visual appearance of the drill core for analysis by X-ray computed tomography and micro-XRF.

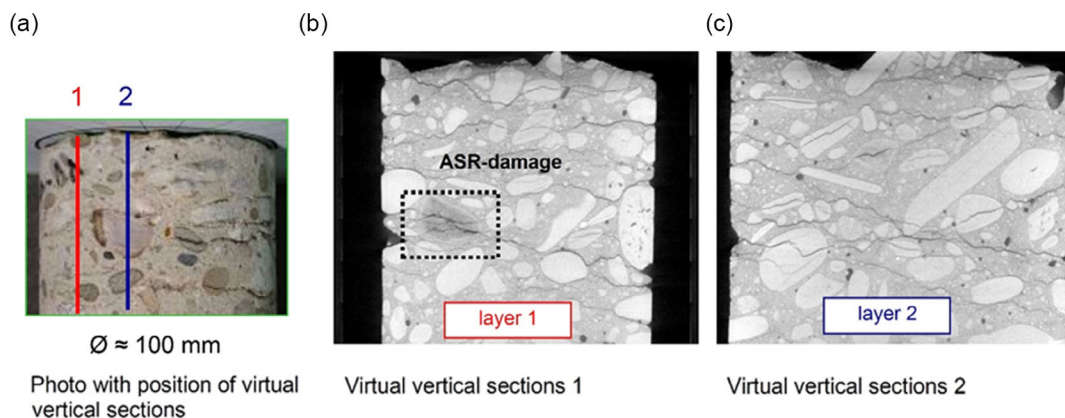


Figure 19. Selected images of a severely damaged drilling core and its microstructure in two sections as computed with 3D CT (the frame in layer 1 tags an aggregate grain with many cracks) based on ref. [93] a) Photo with position of virtual vertical sections. b) virtual vertical sections 1, c) virtual vertical sections 2.

cryptocrystalline quartz and chalcedony. ASRP is visible as a rim around the grain and within some cracks of the grain extending into the cementitious matrix. The element distribution mappings acquired by micro-XRF (**Figure 20**) can be used to validate that the rims around the grain visible in the microscope consists of ASRP, as it is associated with a relative enrichment of potassium. The high concentrations of sulfur in the cracks surrounding the grain are remarkable and further analysis with SEM/EDX confirmed that this phase is ettringite. The formation of secondary ettringite in the context of ASR is a well-known phenomenon. The debate about the reaction sequence and the associated contribution to damage is on-going in the scientific community,^[94–98] but in the case study presented here it was concluded that the cracks on both micro- and macroscale were mainly induced by ASR.^[93]

In summary, the combined use of various innovative and traditional testing techniques proved to be very effective in determining the causes of damage in the laboratory. Not only the cracks but also the decomposition of aggregates caused by the ASR could be visualized spatially in the drilled cores. 3D-CT enables a selection of suitable regions for the preparation of polished thin sections for microscopic and microchemical investigations. The large-scale elemental distribution images obtained with micro-XRF on these sections proved to be very useful for

identifying ASR damage with accompanying secondary ettringite formation.

4.2. ASR Damage Analysis from Pop-Outs on a Foundation Slab of a Car Park

A foundation slab of an underground car park was investigated because the concrete showed severe spalling (pop-outs). The pop outs in the concrete surface had a depth up to a few mm and were therefore visible macroscopically. Most of these defects were filled with a polymer-like material and surrounded by white coatings (**Figure 21a**). The ductile material filling the holes seemed to be amorphous and gel-like, prompting the initial suspicion that an ASR-sensitive aggregate type could be the reason for the damage.

A thin section was prepared from a drilled core for further evaluation. Using optical microscopy (**Figure 22**) combined with micro-XRF (**Figure 23**), the visible damage could be clearly attributed to ASR. It could be proven by microscopy of the thin sections that alkali-sensitive flint aggregates were used. Strong dissolution processes in the sensitive aggregate, associated with massive gel formation, were identified.

The subsequent expansion of aggregates located close to the surface caused the characteristic pop-outs. The elemental

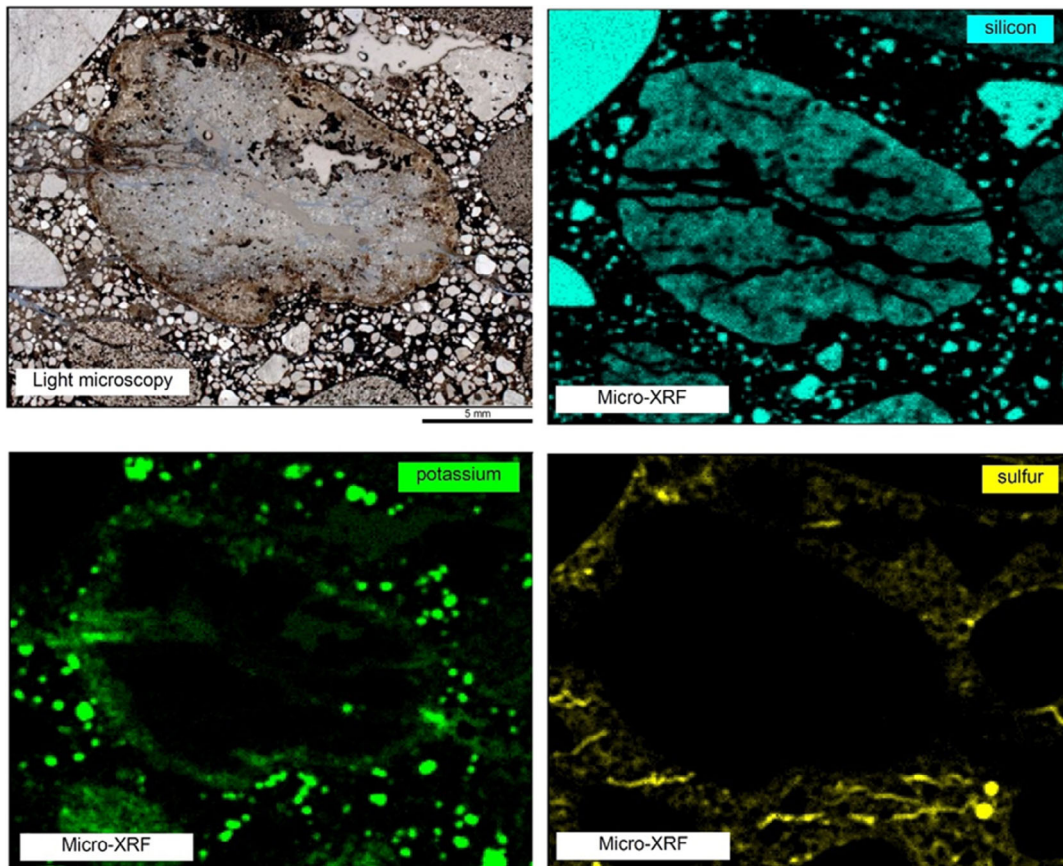


Figure 20. Cracked aggregate in a thin section: result of the microchemical investigations with micro-XRF, indicating potassium enrichment associated with ASR in the rim of the grain, and secondary ettringite formation in cracks based on ref. [93].

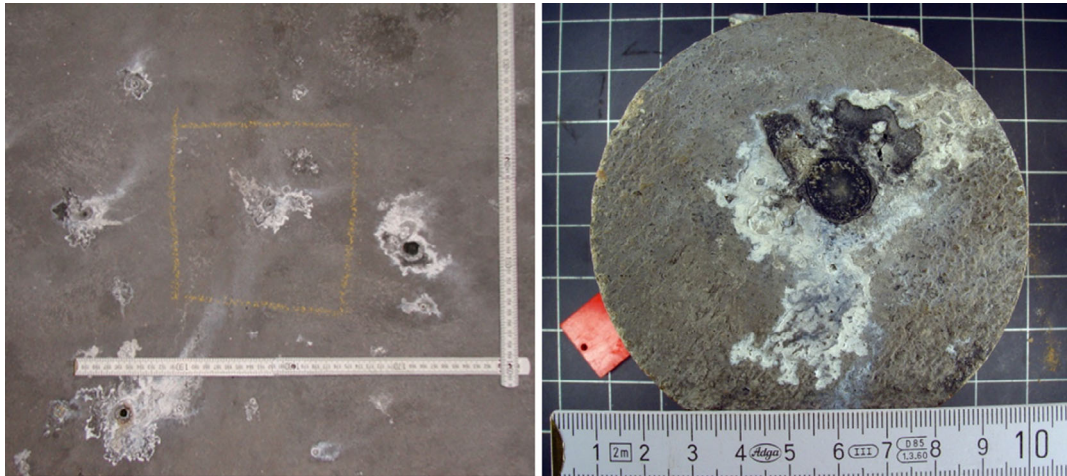


Figure 21. Validation of ASR as the cause for the deterioration of a foundation slab in an underground car park: a) macroscopic damage pattern; b) top view of drilling core extracted for further examination.

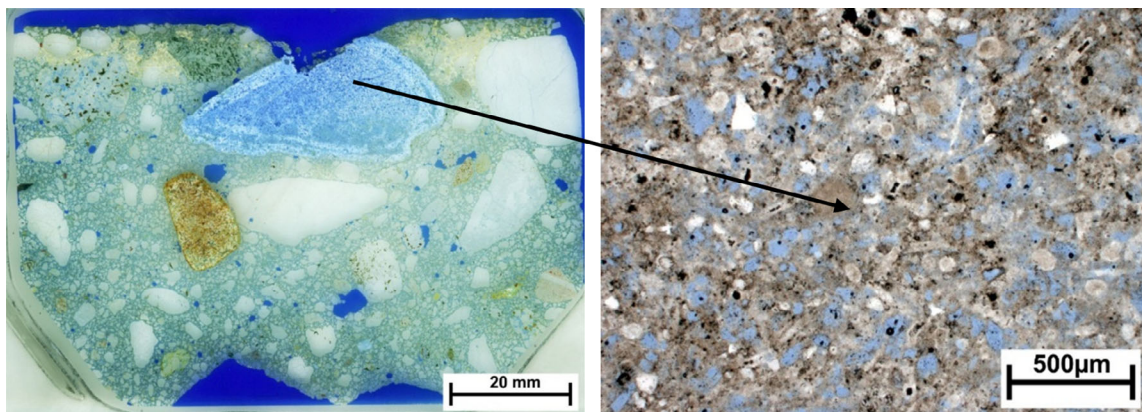


Figure 22. Validation of ASR as the cause for the deterioration of a foundation slab in an underground car park by microscopic investigation: a) thin section overview from drilling core vertical cut; b) detailed view from the high reactive chart.

composition of the gel-like material was obviously sodium enriched, which led to the assumption that the ingress of further alkalis from deicing salts supplied by parking cars in winter contributes to the intensive damage. The deterioration of the concrete surface thereby speeds up the process of deterioration. The white covering on the surface consists of crystallized, presumably carbonized ASRP which is characterized by an increased sodium content compared to the amorphous gel.^[99]

4.3. Characterization of ASR Products by Means of Raman Spectroscopy

Due to the complex boundary conditions within the concrete matrix, which vary depending on the countless mixture concepts and development processes, the interrelationships between the chemical composition and the mostly amorphous structure of the ASRP and the parameters that influence them are not yet fully understood. Results from optical microscopy and element mapping (EDX or micro-XRF) indicate microchemical and sometimes also microstructural changes depending on the local

position, the type of rock, and the environment. In recent years, there has been a lot of interest in studies of the chemical composition and microstructural evolution of ASRP by means of Raman spectroscopy coupled with microscopy.^[100–106] Unfortunately, the analysis of ASRP chemical structure in real concrete samples is very complex due to the small volumes of ASRP, their local inhomogeneities, and variabilities.

4.3.1. Investigations of ASRP

The aim of current research at BAM is to derive a systematic comparison of ASRP which forms under different conditions. In this context, local inhomogeneities dependent on the associated surroundings (i.e., in the aggregate, the transition zone, or the cement matrix) as well as time-dependent changes in ASRP will be systematically analyzed. Especially, in the context of accelerated testing, it is of great interest to identify potential differences in ASRP resulting from different temperature and moisture conditions as well as from frost and deicing salt applied during the testing procedure. Correlations between the chemical

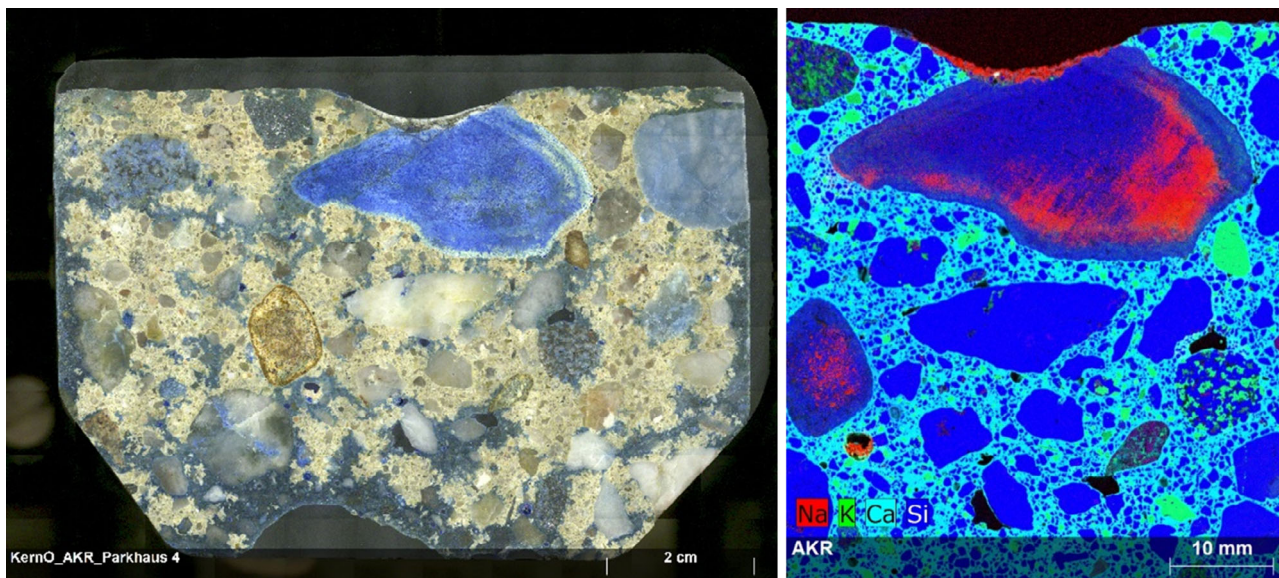


Figure 23. Validation of ASR as the cause for the deterioration of a foundation slab in an underground car park by microchemical investigation: a) photograph from drilling core vertical cut, polished sample; b) elemental distribution analyzed by micro-XRF.

composition or structure of ASRP and the specific conditions applied during accelerated testing could help to gain new insights into the detailed mechanism of deterioration and help to make accelerated tests more representative for individual cases.

No special sample preparation for Raman spectroscopy is needed. In order to exclude the possible influences of water, the specimen sections are prepared without the use of water. The pores or cracks are then examined for potential ASRP fillings by stereomicroscopy and representative locations are analyzed by Raman spectroscopy (see **Figure 24**). Subsequently, the spectra are normalized, smoothed, and the background is subtracted by

using Origin Pro 2021. The main characteristic vibrational bands in the range of $400\text{--}800\text{ cm}^{-1}$ and $800\text{--}1200\text{ cm}^{-1}$ represent the Si—O—Si and Si—O bonds of the SiO_4 tetrahedra. The symmetric bending vibration at around 600 cm^{-1} is assigned to Q^2 species. The symmetric stretching vibrations at around 1020 cm^{-1} and around 1070 cm^{-1} are assigned to Q^3 and Q^2 species.^[101,107]

4.3.2. Feasibility Study on Thin Sections

The aim of a first exploratory study was to elaborate the potential of Raman spectroscopy to identify differences in the chemical composition and microstructure of ASRP in concrete thin

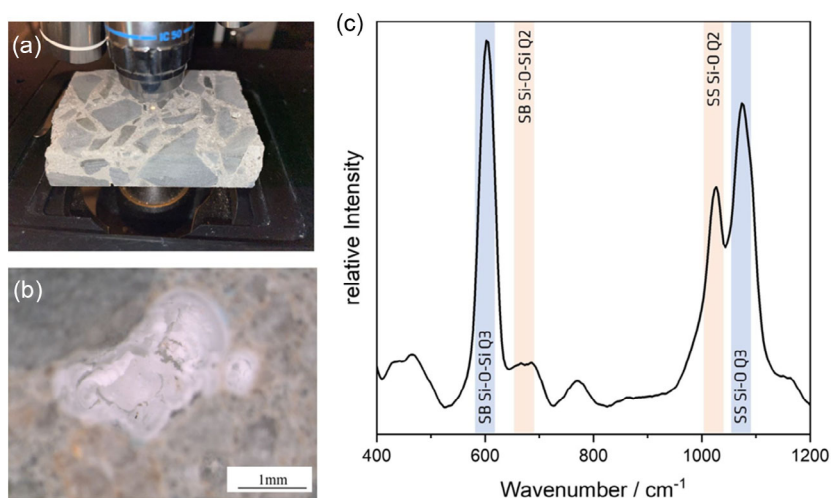


Figure 24. a) By microscopy of a concrete section b) a pore filled with ASRP is identified and c) within this focus a Raman spectrum of ASRP is recorded. The ASRP shows typical symmetrical bending vibrations of Si—O—Si bonds at around 600 cm^{-1} assigned to Q^3 species and symmetrical stretching vibrations of Si—O bonds at around 1020 cm^{-1} and around 1070 cm^{-1} assigned to Q^3 and Q^2 species, respectively.

sections, depending on the local position in the surrounding microstructure. Specific emphasis was placed on the documentation of changes observable with the progression of the ASRP from the aggregates into the cementitious matrix. The thin sections were prepared from drill cores of 10- to 20-year-old concrete highway pavements taken in the context of the investigations described in Section 5.1. The main aggregates of the concrete in this study were alkali-silica reactive rhyolite and quartzite. Whereas some of the drill cores already exhibited damage typical of ASR, others showed the characteristic deterioration only after the additional application of an accelerated testing procedure.^[100]

After identification of the ASRP by means of polarized light microscopy, Raman spectroscopy was applied to gain further information. The spectral range of 300–850 cm^{-1} was extracted from each Raman spectrum. The evaluation was carried out semiquantitatively based on the peak fit and the resulting normalized integrated areas of the different vibrational bands using fityk 1.3.1 software.^[63] To obtain the chemical composition, the same spots on the samples were analyzed with SEM (in this case in the context of a master thesis cooperation with the University Potsdam: LEO1530 VP (ZEISS) coupled with EDX, which was performed at 15 kV and 2 mA beam current with 100 live seconds counting time). The concentrations were calculated with ZAF corrections. Natural silicates and oxides were used as standards.

The results are presented as a case study using two different thin sections. The thin section of sample A originates from a drill

core that showed signs of ASR directly after removal. It reveals several cracks with one crack running along the edge of a quartzite aggregate. At one end it branches out in the cementitious matrix while on the other side the crack stops directly at the border between aggregate and cementitious matrix (Figure 25a). The microscopic investigation of the thin section did not reveal the ASR starting point. After the combined analysis with SEM/EDX and Raman spectroscopy, the point of crack branching can be assumed to be the origin of the ASR. In agreement with the results of ref. [108], the Ca/Si ratio measured by SEM/EDX slightly increases from 0.25 to 0.36 with progressive distance from the origin of the ASR product (Figure 25c) while the evaluation of the normalized Q species analyzed by Raman spectroscopy indicates evolution from an ASR gel with a chain-like (Q^2) and layered (Q^3) structure to a C–S–H phase indicated by an increase of $Q^2_{\text{C-S-H}}$ species (Figure 25b). The plot of the (Na + K)/Si ratio along the crack shows no clear trend (Figure 25d), which can be traced back to the fact that the EDX measurement is not as sensitive to light elements (Na, K) as the wavelength dispersive X-ray (WDX) analyzer of a microprobe.

The thin section of sample B originates from a drill core which exhibited first signs of ASR only after application of the cyclic climate storage test described in Section 3.5.2. Microscopic investigation identified a crack within a rhyolite which runs through the cementitious matrix and ends in a pore, and which is partly

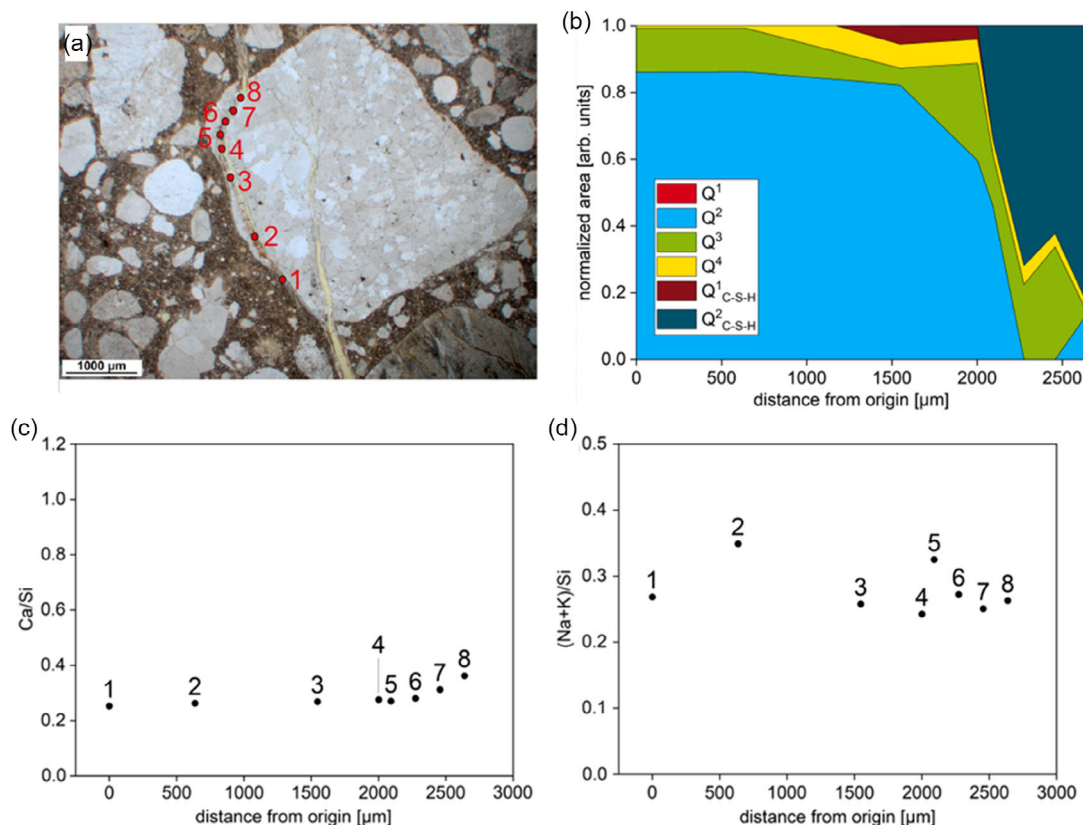


Figure 25. Chemical and microstructural analysis of sample A with quartzite aggregate: a) microscope image of the thin section with measuring points marked; b) normalized ratio of Q species analyzed by Raman spectroscopy in relating to the distance of the measured points from the origin; c) Ca/Si ratio; and d) (Na + K)/Si ratio determined by SEM/EDX plotted against the distance of the measured point from the origin.

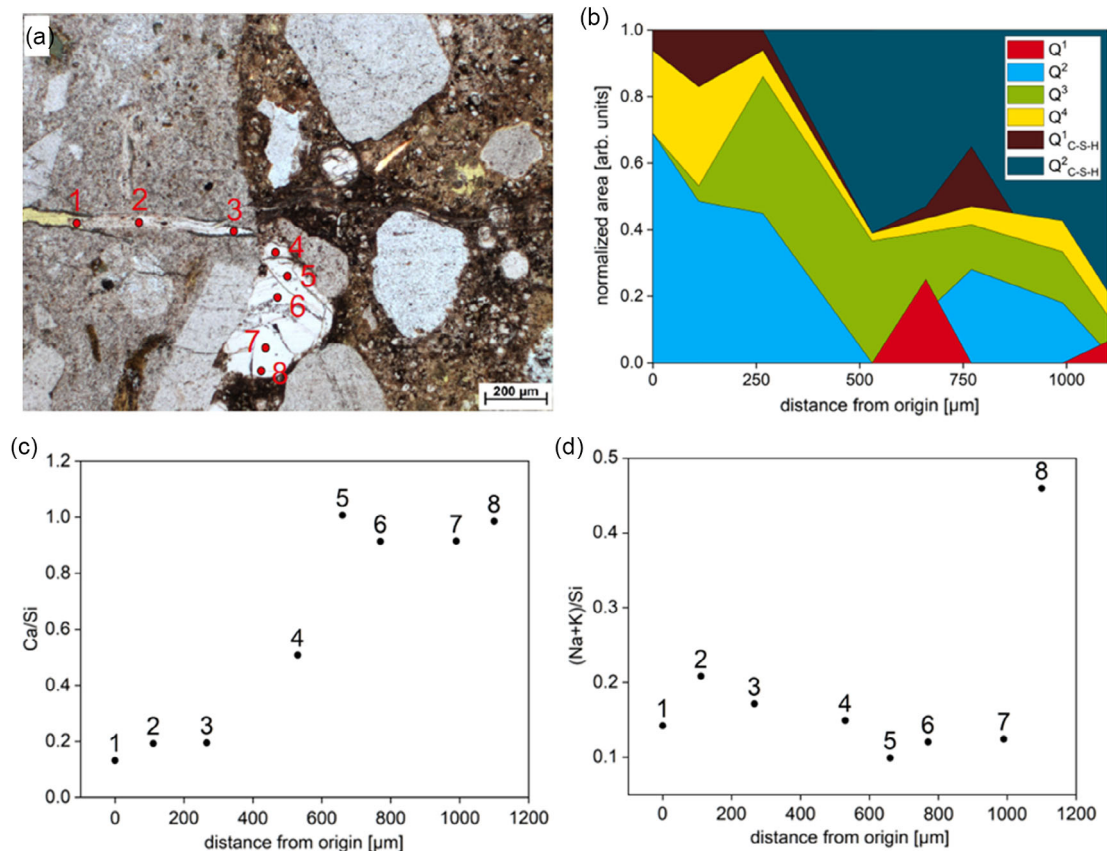


Figure 26. Chemical and microstructural analysis of sample with Rhyolite aggregate: a) microscopy image of the thin section with marking of the measuring points; b) normalized ratio of Q species analyzed by Raman spectroscopy in relating to the distance of the measured points from the origin; c) Ca/Si ratio; and d) (Na + K)/Si ratio determined by SEM/EDX plotted against the distance of the measured point from the origin.

filled with an amorphous material (Figure 26a). The evaluation of the normalized Q species reveals the distinct progression from an ASR gel with a chain-like structure (Q²) to a layered structure (Q³) and in the last step the transformation to a C–S–H phase indicated by an increase of Q²_{C–S–H} species (Figure 26b). The trend that could already be seen from the systematic change in the Q species is supported by the significant increase in the Ca/Si ratio from about 0.2 to 1.1 with increasing distance from the origin of the reaction in the aggregate (Figure 26c). The (Na+K)/Si ratio exhibits only small changes to lower alkali concentrations with advancing crack length (Figure 26d). The average Ca/Si ratio of amorphous and crystalline ASRP is specified between 0.21 and 0.26 by Shi and Lothenbach^[108] and Hou et al.^[109] while the average Ca/Si ratio of C–S–H phases is 0.8.^[110] Corresponding to this development, the structure of the ASR product is first dominated by Q² species which represent a chain-like structure^[58,101,102,107,111] and later by Q²_{C–S–H} species which represent the chain-like structure of C–S–H phase.^[112] The fact that the Ca/Si ratio exceeds the average value of 0.8 at the last measurement points is probably due to the storage at a temperature of 60 °C and the immersion in NaCl solution where more Ca dissolved from the cementitious matrix and precipitated as C–S–H phase.

The exemplary results of this study show that the use of Raman spectroscopy in addition to SEM/EDX provides valuable information for the spatial and temporal characterization of the chemical and structural composition of ASRP. It also shows that it is possible to determine the origin of the ASR and to monitor its development in the cementitious matrix. In particular, the boundary conditions of the test procedure that defines the environment for the development of the ASRP appear to be reflected in the analysis of the reaction products. However, these are preliminary results that need to be validated.

In general, the reaction products show an increasing Ca/Si ratio with progressive crack length. An ASRP originating from an aggregate and running through the cement paste is characterized by a high initial (Na + K)/Si ratio which decreases with increasing distance from the origin. This supports the hypothesis that with distance and probably time, more Ca gets incorporated from the surrounding cement paste.^[58,101,109,113,114]

The reaction product with a high (Na+K)/Si ratio is more likely to be in a swellable state and may develop into a less or nonswellable state with progressive crack length.^[105] The increase of the Ca/Si ratio leads to a distinct depolymerization of the gel and thus conversion of the structure, which is manifested as an increase of Q species that account to C–S–H

phases.^[102] The reaction products with low Ca/Si ratio can be allocated to initial products formed inside aggregates, whereas the high Ca/Si ratio mostly develops outside the aggregate within the cementitious matrix.

5. Concrete Road Pavements—Multimethod Investigations and a Novel ASR-Avoidance Strategy

A central research focus of BAM in the ASR field over the past 15 years has been on concrete pavements. This is because increasing amounts of ASR-associated damage to concrete pavements occurred in the German highway network (BAB) during this period. According to a nationwide analysis of the German highway network carried out by the Federal Highway Research Institute (BAST) in 2012, ≈ 1500 km carriageway were suspected of ASR.^[115] In practice, this type of damage can reduce the service life of the concrete pavement from 30 to 10 years in some cases.

In view of this, research activities range from developing a test methodology for analyzing the condition of existing concrete pavements where ASR is suspected,^[116,117] to analysis of the influence of selected factors on ASR. This includes simultaneous cyclic stress and supply of deicing salt^[118–126] and the solubility of alkali-sensitive aggregates in the presence of NaCl.^[127,128] Furthermore, a novel ASR avoidance strategy was evaluated.^[129,130] Selected aspects are presented in the following subsections.

First, Section 5.1 presents a method for analyzing the condition of existing roads where ASR is suspected. An essential element is damage classification by visual examination of the relevant pavement section. Dark discoloration of the surface at the slab edges is taken as the initial damage indicator. This is assumed to be due to increased moisture in the concrete edges. To test this hypothesis experimentally in situ, a nondestructive test combination is presented in Section 5.2, based on the general ASR damage classification according to Angerer.^[131]

In addition to the visual check and evaluation of damage indicators, the analysis of deicing salt penetration is a core element of the damage analysis. Therefore, Section 5.3 presents LIBS (see Section 2.5), as an innovative test method that provides analysis of deicing salt penetration.

Finally, Section 5.4 gives an insight into current research at the BAM into ASR avoidance strategies. This section presents initial findings on examining the performance of internal hydrophobization, a novel ASR avoidance strategy for concrete pavement.

5.1. Testing Methodology for Existing Concrete Pavements

Over the last 10 years the BAM carried out condition and damage analyses on ≈ 70 sections of the German highway network with different degrees of ASR damage.^[116,117,132] The highway sections to be analyzed were selected on the basis of inspections in 2012 comprising visual assessment of the pavement surface of all federal highways made of concrete. The intention was to find answers to the following questions for each of the highway

sections examined: 1) To which ASR damage category should the visual damage be assigned? 2) Is ASR present and how serious is it? Is the ASR overlaid by delayed ettringite formation (DEF)? 3) How deep does the deicing salt penetrate the concrete pavement? 4) What is the ASR residual damage potential and thus the remaining useful life of the concrete pavement?

The test program shown in Figure 27 was developed and applied to answer these questions.

5.2. Analysis of Damage Category “Darkening of the Road Surface”

According to Angerer,^[131] damage to the concrete pavement due to ASR originates in the upper layer of the top course concrete and typically evolves through three damage categories (DC) as shown in Figure 28. First, darkening of the concrete surface appears near the transverse joints (DC I-O) that is associated at a later stage with increased cracking (DC II-O). This is followed by breakouts near the joints (DC III-O).

5.2.1. Test Methodology

To verify the role of moisture in darkening of the concrete pavement surface (DC I-O), moisture distribution in a representative pavement slab was examined in situ in two stages, using nondestructive testing methods. In the first step, radar was used to analyze the lateral distribution of the integral moisture content over the depth of the pavement slab over a wide area. The second step was to determine moisture distribution in the upper concrete boundary zone along selected measurement lines using ¹H-NMR with in-depth resolution. The NDT findings were then validated using the gravimetric loss-on-drying method on drill dust samples taken from a range of depths. A brief description of the measurement principle and the application of the NDT methods used can be found in Section 2.6 and 2.7.

5.2.2. The BAB Highway Section Examined

Figure 29 gives a visual impression of the external appearance of the two sample concrete slabs on the A 113 highway. The darkening of the pavement surface can be clearly seen, mainly near the transverse joint and the joint intersection. The BAB section examined can be classified between damage categories DC II-O and DC III-O due to the very distinct cracking around the joint intersection. This highway section was constructed in 2004 as a full course two lift construction. The concrete pavement is ≈ 27 cm thick and is separated from the ≈ 20 cm thick compacted subbase course by nonwoven geotextile fabric. The tests took place after this highway section had been in use for 12 years.

5.2.3. Findings and Discussion

Figure 30 gives an overview of the radar findings. The starting point is the top view of the BAB section with the radar measurement field marked in red (Figure 30b). Figure 30a shows a sample image of a D scan gained by taking a cross section of the data cube vertical to the direction in which the antenna pair was moving. It can be seen that near the transverse joint the time

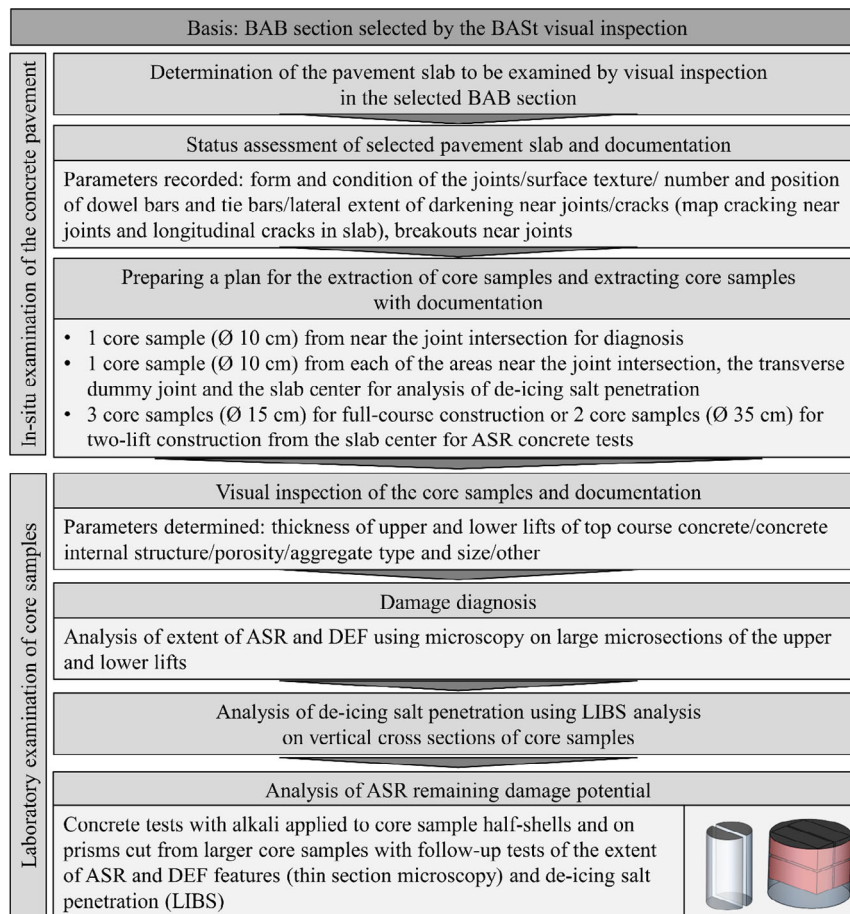


Figure 27. Test methodology for condition and damage analysis of existing concrete pavements with suspected ASR.

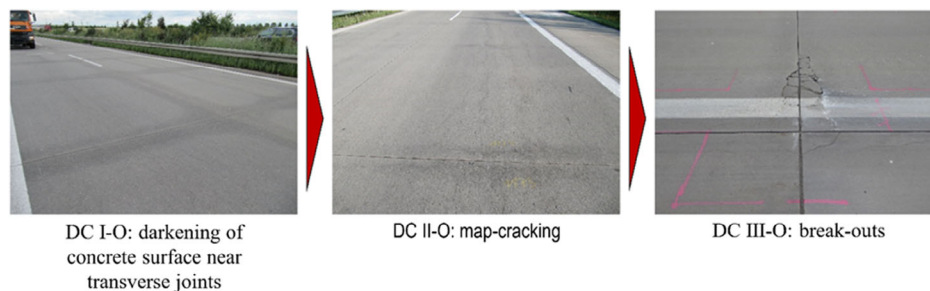


Figure 28. Evolution of ASR damage on the surface of concrete pavement caused primarily by the top layer of concrete. Adapted with permission.^[115] Copyright 2018, Ernst & Sohn. a) DC I–O darkening of concrete surface near transverse joints. DC II O map-cracking, DC III-O: Break Outs.

of flight taken by the radar pulses between surface and back wall of the concrete pavement increases by approximately 0.4 ns. The lateral extent of the area where the times of flight increase, starting from the transverse dummy joint, correlates with the darkened area of the concrete surface. The increased time of flight between surface and back wall of the concrete pavement leads to the conclusion that the integral moisture content of the concrete pavement is greater near the joints, taking into account the maximum variation in thickness of ± 5 mm of the concrete

pavement as determined by core samples. The C scan taken at a depth of 27.5 cm confirms this conclusion. The C scan shows that the reflection of the pulse at the back wall of the concrete slab is not yet present. It should be noted that the similar intensities of the reflected signal in the lower center of the C scan (area outlined in red; Figure 30c) to those in the joint area represent artifacts. They are caused by the scanner, that is, by the differences in distance between the radar antennae and the concrete surface.

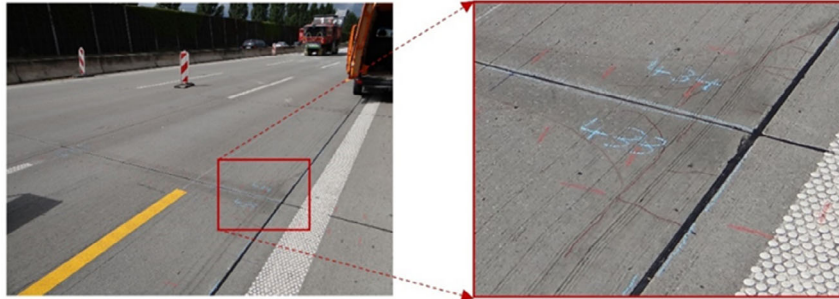


Figure 29. Visual appearance of the motorway section. Adapted with permission.^[115] Copyright 2018, Ernst & Sohn.

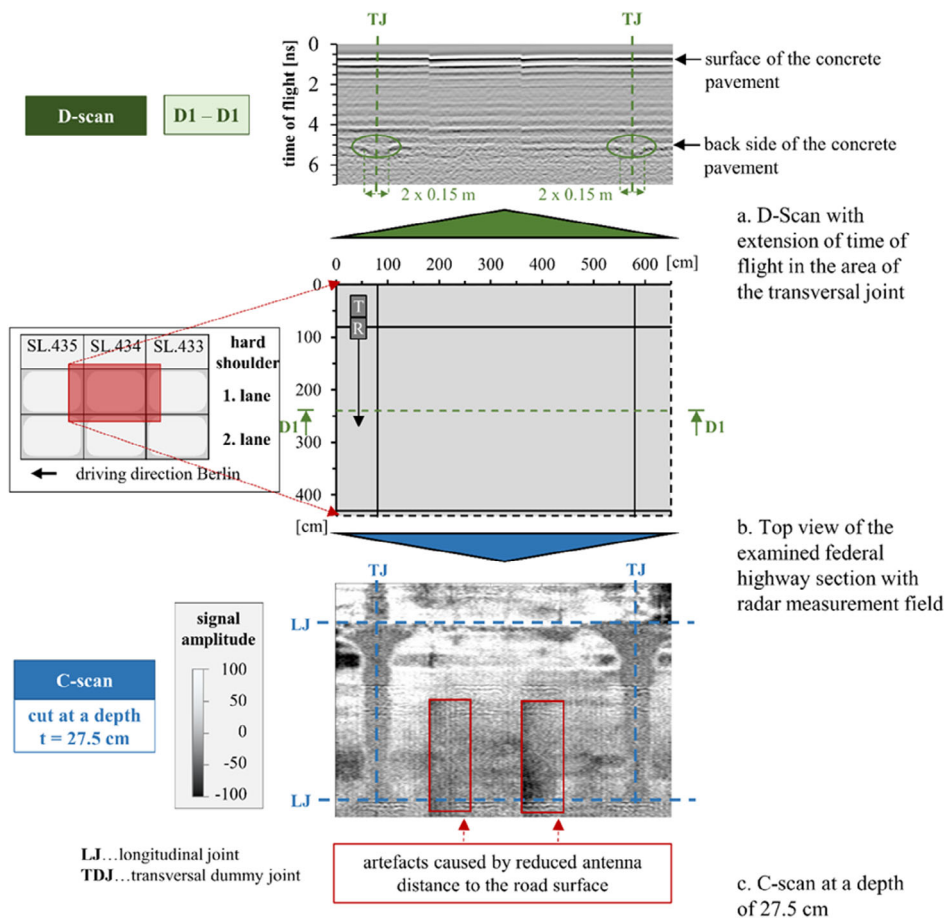


Figure 30. Result of the integral moisture measurements in concrete using radar. Adapted with permission.^[115] Copyright 2018, Ernst & Sohn. a) D-scan with extension of time of flight in the area of the transversal joint. b) Top view of the examined federal highway section with radar measurement field. c) C-scan with a depth of 27.5 cm.

The radar test findings are supported by the NMR results. **Figure 31** shows the findings of moisture content measurements using the NMR mouse at certain points along one measurement line in each of three depths in the concrete boundary zone. First, **Figure 31a** shows the moisture content in the concrete boundary zone along a measurement line starting at the joint intersection. Second, **Figure 31b** gives an adequate depiction starting from the

transverse dummy joint in the middle of the first traffic lane. In both diagrams, the lateral extent of the darkened pavement is shaded grey, to visualize the correspondence with the discoloration. It can be seen in both diagrams that increased NMR amplitudes and therefore increased moisture content in the concrete boundary zone is concomitant with the darkening of the pavement surface. The tendency to higher NMR amplitudes in the

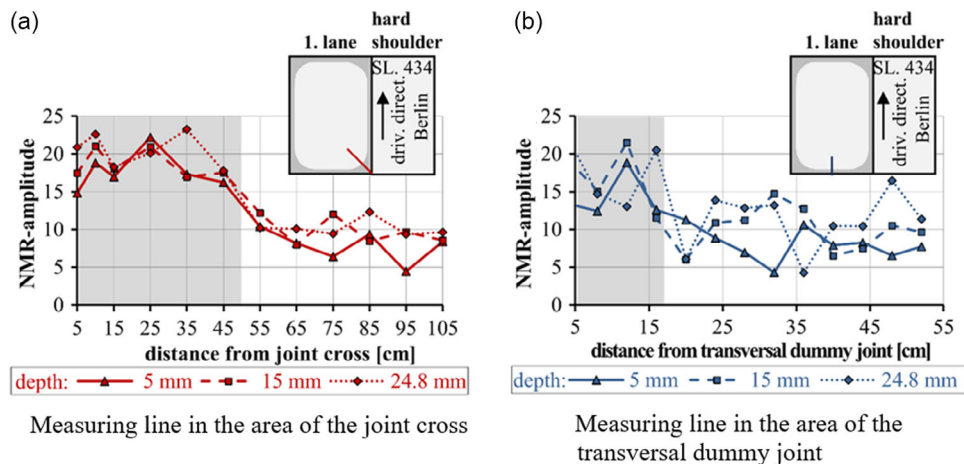


Figure 31. Results of NMR moisture measurements at selected depths in the concrete boundary zone along two measurement lines: a) measuring line in the area of the joint cross; b) measuring line in the area of the transversal dummy joint. Adapted with permission.^[115] Copyright 2018, Ernst & Sohn.

joint intersection area than in the transverse dummy joint area also indicates higher moisture penetration in the concrete boundary zone.

5.2.4. Conclusion

The two-stage in situ tests using nondestructive testing methods give the first experimental confirmation of the working hypothesis stated at the beginning; that increased moisture penetration in the concrete causes darkening of the concrete pavement surface near the joints. First, the large-scale radar analysis showed increased times of flight for the radar pulses between the surface and back wall of the concrete pavement near the transverse dummy joints and the joint intersection. This indicates increased integral moisture content in the concrete pavement. It also clearly shows that the increased moisture penetration near the joints reaches its greatest lateral extent near the joint intersection. The more detailed NMR moisture measurements in the concrete boundary zone show a good level of correlation between higher NMR amplitude, indicating greater moisture content and the darkened surface of the concrete pavement near the joints. Further detailed information on analyzing the causes of the initial ASR damage leading to darkening can be found in the study by Weise et al.^[115]

5.3. Analysis of Deicing Salt Penetration Using LIBS

To demonstrate LIBS' effectiveness, the following section describes tests carried out on core samples from the section of BAB highway A 113 already examined in Section 5.2 in relation to darkening of the concrete. To verify the influence of the core sample extraction site, a vertical section of the upper core sample segment (\varnothing 10 cm) from the center of the slab and one from near the transverse dummy joint were examined and compared (**Figure 32**). To assess the quality of the LIBS measurements, comparative wet chemical analyses were carried out on core sample segments cut parallel to the pavement surface (height: 1 cm) as set out in the German Committee for Structural Concrete (DAfStb)'s Booklet 401.^[133] The sodium content of the filtrate was quantitatively analyzed using optical emission spectrometry with inductively coupled plasma (ICP-OES) and the chloride content was quantitatively analyzed using potentiometric titration. A brief description of the LIBS measurement principle can be found in Section 2.5.

5.3.1. Measuring Regimes, Measuring Parameters, and Calibration

The image in Figure 32 of the dry cut sample surface to be examined by LIBS was scanned by laser in a meandering line without

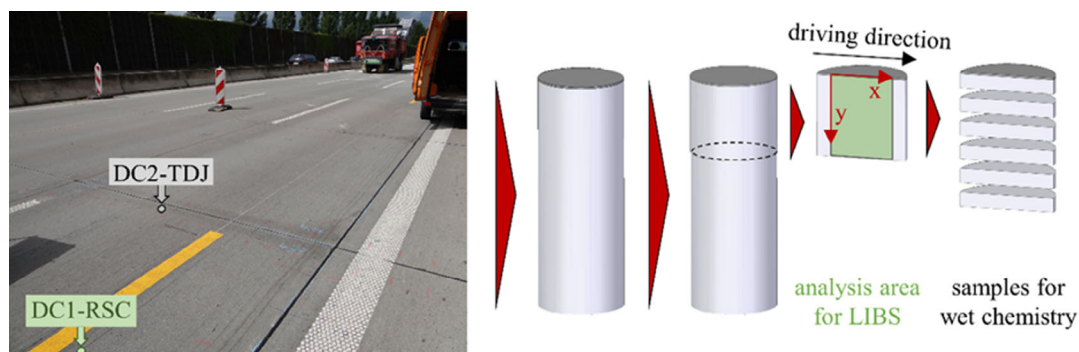


Figure 32. Sampling locations of the drilling cores (left) and cutting plan (right). Adapted with permission.^[80] Copyright 2018, Ernst & Sohn.

further preparation. The measured surface was 90 mm × 60 mm in size. The distance between measurement points was set at 0.5 mm in x and y directions. At each measurement point, six short high-energy laser pulses were applied (energy: ≈ 300 mJ, duration: ≈ 1.5 ns). The spot diameter was approximately 100 μm . The measurement time for a surface scan was 0.5 h. The calibration necessary for quantification was carried out in accordance with DIN 32645. It was based on cement stone prisms made from Portland cement and mineralized water with a water/cement ratio of 0.5 and a defined application of NaCl. After 28 days of defined preconditioning, the prisms were broken and ground to homogenize Na and Cl distribution. The resulting powder was subjected to wet chemical analysis and in parallel compacted into samples for the LIBS analysis. During calibration for sodium and chloride, the LoD was determined at 0.02 and 0.03 wt% and the limit of quantification (LoQ) was determined to be 0.05 and 0.09 wt%, both as statistical values. Further information on this calibration can be found in previous studies.^[80,134–136]

5.3.2. Findings and Discussion

As an example, **Figure 33** shows the typical result of a large-scale imaging Na and Ca analysis using LIBS for the upper segment of the core sample from the center of the slab (DC1-RSC). The intensity of the LIBS signal is color-coded in each case. Figure 33 also shows the procedure for determining the Na depth profile from the Ca and Na area scan including aggregates. The Na area scan seen here clearly shows that the aggregates contain

a high amount of sodium. When the calibrated LIBS measuring signals are accumulated and averaged along the individual horizontal measurement lines, this high sodium content results in a very undifferentiated image of the Na depth profile that does not adequately reflect deicing salt penetration in the concrete pavement. Because the sodium in the aggregate falsifies the depiction of how the deicing salt is primarily transported through the cement matrix, the aggregates were identified and eliminated by using the significantly higher calcium content in the cement matrix compared to the aggregates, which can be clearly seen in the Ca area scan with aggregates (Figure 32). The Na depth profile generated after eliminating the aggregates, as shown in the Na area scan, gives a plausible description of deicing salt penetration into the concrete pavement. It shows a gradient rising from the surface to the interior of the pavement that indicates a minimum sodium penetration depth of ≈ 15 mm. The Cl depth profile was determined in the same way.

Figure 34 shows a comparative presentation of the Na and Cl depth profiles determined by LIBS and by wet chemistry in the core sample from the slab center (DC1-RSC) and near the transverse dummy joint (DC2-TDJ). It should be noted that to evaluate the accuracy of the LIBS method, bars are present in the diagrams that mark the area below the LoQ of the LIBS process for the Na and Cl content. The depth profiles determined by LIBS show that sodium penetrates to a depth of at least 15 mm near the transverse dummy joint and similarly in the slab center. In contrast, a greater minimum penetration depth of chloride, ≈ 20 mm, was determined in both slab areas. The slight increase in chloride content at a depth of 55–80 mm is probably

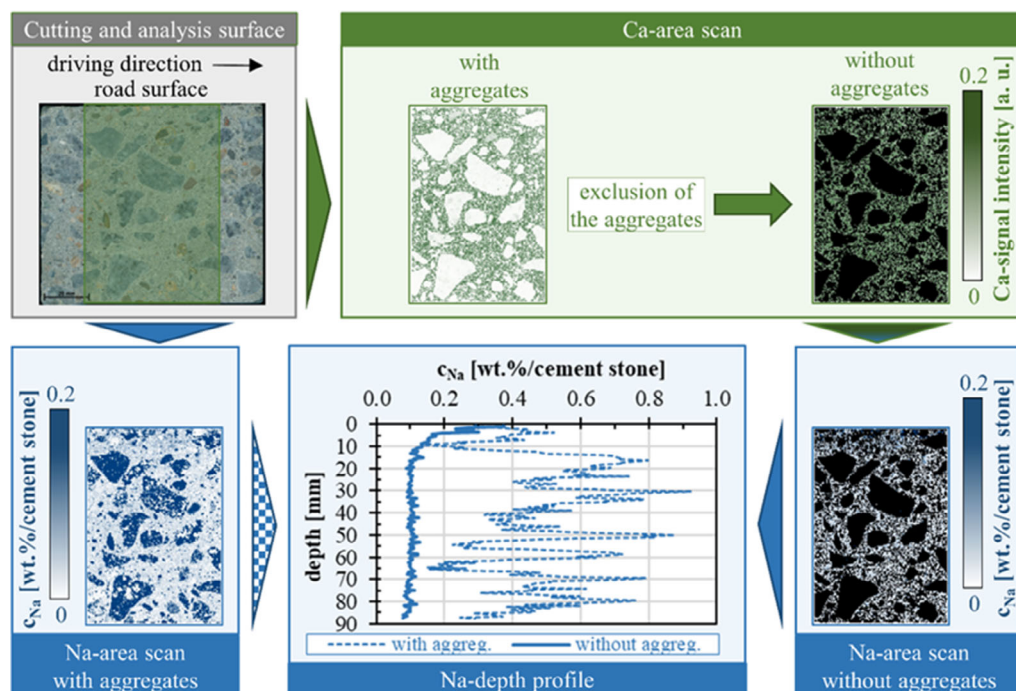


Figure 33. Procedure for determination of the sodium content relative to depth based on the evaluation of the LIBS area scan data using the Ca-exclusion criteria for the elimination of aggregates. The upper segment of a drilling core taken from road slab center (DC1-RSC) is used as an example. Adapted with permission.^[80] Copyright 2018, Ernst & Sohn.

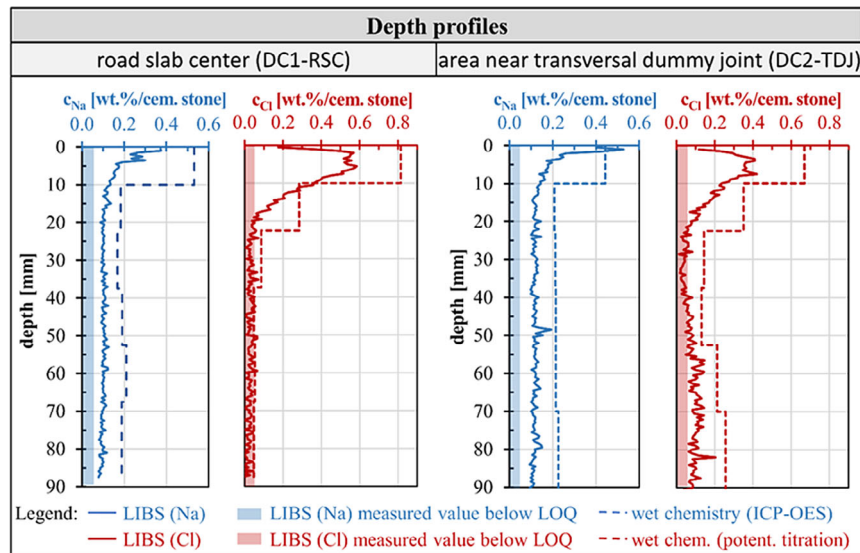


Figure 34. Comparative depiction of sodium and chloride contents relative to depth for drilling cores taken from the center and the edge of the concrete pavement slab.

due to chloride ingress from the side via the transverse dummy joint. In the adequate sodium depth profile, this phenomenon is not present.

The Na and Cl depth profiles determined for both core samples by wet chemistry and by LIBS show a good qualitative agreement. As expected, the local depth resolution of the Na and Cl penetration front is significantly greater in the LIBS measurements than in the integral wet chemical analysis of the individual core sample segments. The quantitative comparison of the Na depth profiles in the cement stone determined by LIBS and by wet chemical analysis shows, however, that the sodium content determined by wet chemical analysis with in-depth resolution is higher than that determined by LIBS. One possible explanation could be that sodium dissolved out of the aggregate when the existing concrete was dissolved with diluted nitric acid. It should also be noted that the LIBS and wet chemical analysis took place at different local measurement areas. This latter probably explains the partially higher chloride content determined by wet chemical analysis in the core sample from near the transverse dummy joint. Further tests are essential in order to evaluate the suggested explanations.

To sum up, it can be stated that LIBS can determine deicing salt penetration in concrete pavement with significantly higher spatial resolution and much more quickly than wet chemical analysis. It was also shown that to determine the Na depth profile from the Na area scan, it is essential to eliminate the aggregates using Ca exclusion criteria. The Na depth profiles determined by LIBS in this way correlate qualitatively with those determined by wet chemical analysis. Testing the suggested explanations for the quantitative discrepancies between the two processes is a topic for further research. Further detailed information about determining deicing salt penetration in concrete pavements with additional use of micro-XRF, described in Section 2.4, can be found in the study by Weise et al.^[80]

5.4. Evaluation of Internal Hydrophobic Treatment of Road Pavement Concrete as a Novel Preventive Measure Against Alkali Aggregate Reaction

Following the above insights into selected aspects of the test methodology for the condition and damage analysis of concrete pavement with suspected ASR, we now focus on avoiding ASR in newly constructed concrete pavement. The normative national procedure for avoiding the use of alkali-sensitive coarse aggregate in new concrete pavement was explained in detail in Section 3.8. Eight years of practical experience with this regulation, however, have shown that it significantly restricts the range of coarse aggregates that can be used for concrete pavement. The following section presents internal hydrophobization as a novel ASR avoidance strategy that aims to make borderline alkali-sensitive coarse aggregates usable for concrete pavement.

In contrast to surface hydrophobization, which is already used in road construction, the hydrophobing agent for internal hydrophobization is added during the mixing process of the road pavement concrete. The hydrophobization of the hardened pavement concrete is intended to minimize the moisture and deicing salt input and thus significantly reduce the ASR damage process. In contrast to surface hydrophobization, internal hydrophobization also reduces moisture and deicing salt penetration through the joints. The investigations were carried out as part of an already completed research project funded by the BAST.^[129] In this project, three hydrophobing agents with different active agents were used in two different pavement concrete mixtures. In the following, the performance of a silane/siloxane-based hydrophobing agent^[137] in a top concrete designed as an exposed aggregate with a very alkali-sensitive graywacke is shown as an example. Based on the normative requirements, all fresh and hardened concrete properties are considered holistically. The basis for this is provided by Weise et al.^[129,130]

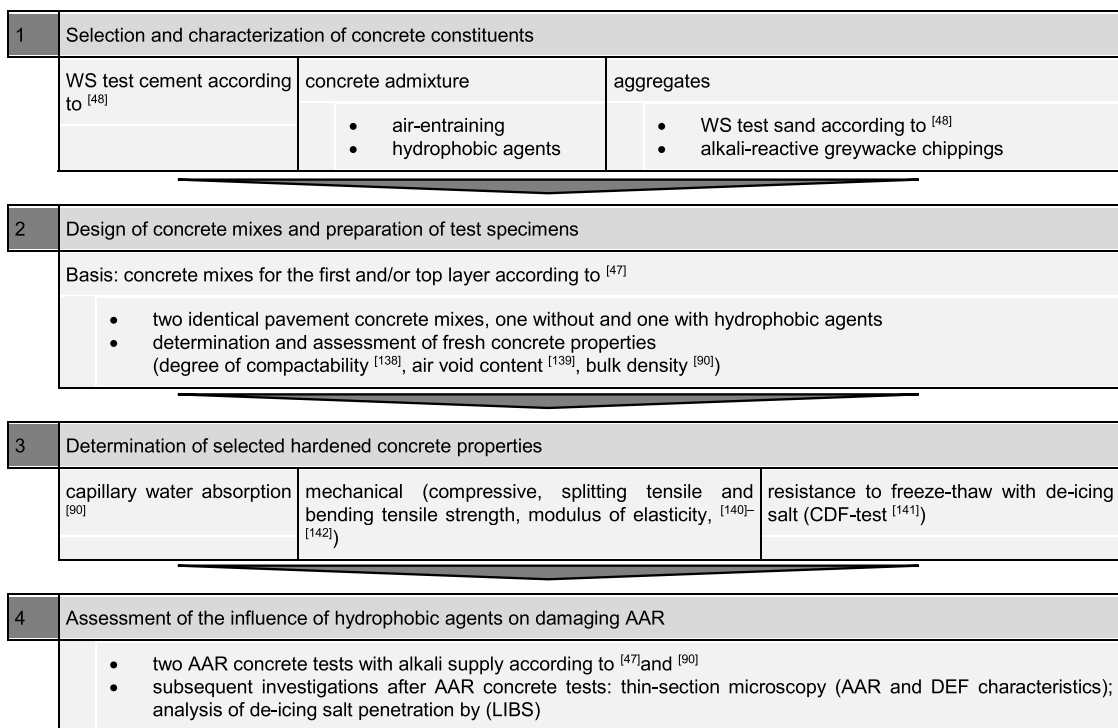


Figure 35. Test program for evaluating the performance of internally hydrophobic pavement concretes. ^[47,90,138–142]

Table 2. Content of concrete mixture.

Type of exposed aggregate concrete	Component							
	Cement [kg m ⁻³]	Water to cement ratio	Air entrainment agent	Hydrophobic agent	Aggregates			
					Sand	Graywacke		
wt% Related to cement mass					0.1/0.5	0.5/1.0	1.0/2.0	2/5
Reference	430	0.45	0.18	–	12	10	8	40
Hydrophobic	430	0.45	1.10	2	12	10	8	40

5.4.1. Global Approach and Concrete Formulations

Figure 35 schematically shows the global procedure for verifying the performance of internal hydrophobization for different types of road pavement concretes.

Table 2 shows the concrete mixtures used to compare the material performances of interest. It is worth noting that a strong interaction between hydrophobic agent (HA) and air entraining agent (AEA) is detected. To ensure the required air void content in fresh concrete with the addition of HA, it is necessary to elevate the dosage of AEA by the factor of ≈ 6 . This is due to the antagonistic effect of the HA and the air entraining agent on the surface tension of the cement paste.

5.4.2. Results and Discussion

Fresh Concrete Properties: By significantly increasing the AEA dosage, the required air void content can be obtained in concrete

with the addition of HA (**Table 3**). The workability does not change significantly when HA is added to the mixture. Air void content and workability can be ensured over a sufficient period of time.

Selected Hardened Concrete Properties: **Table 4** shows the effects of the addition of 2 wt% HA on the hygric and mechanical properties of the exposed aggregate concrete. As expected, the capillary water absorption coefficient is significantly reduced. This ensures the desired reduction of moisture and deicing salt input into the exposed aggregate concrete. The mechanical properties, on the other hand, deteriorate due to the addition of the HA. In the case of compressive and flexural strength, even the minimum 28 d values required by the standards are not reached. It should be noted in this context that both exposed aggregate concrete mixtures without and with hydrophobing were not optimized with regard to the mechanical properties. Therefore, further investigations are required to verify whether conventional concrete technology measures to increase the

Table 3. Fresh concrete properties of each mixture.

Fresh concrete properties			Limit value	Type of exposed aggregate concrete	
				Reference	Hydrophobic
Bulk density	[kg m ⁻³]	10 min	2000–2600 (normal concrete)	2241	2245
		54 min		2254	2242
Air void content	[vol%]	10 min	5.5 ≤ x ≤ 6.5 (ref. to TL Beton Stb 07)	6.4	6.5
		54 min		5.9	6.0
Degree of compactability	[–]	10 min	C1: 1.45–1.26 C2: 1.25–1.11	1.17	1.16
		54 min		1.22	1.22

Table 4. Hardened concrete properties without and with addition of an internal HA.

Properties of hardened concrete			Limit value	Type of exposed aggregate concrete			
				Reference		Hydrophobic	
				Mean	Standard deviation	Mean	Standard deviation
Capillary water absorption coefficient in accordance with standard	[kg (m ² × h ^{0.5}) ⁻¹]	24 h	–	0.41	0.02	0.11	0.08
Compressive strength	[N mm ⁻²]	7 d	–	37.7	2.4	27.1	1.6
		28 d	≥37 ^{a),b)}	40.0	0.9	30.3	0.3
		180 d	–	44.7	0.5	37.7	1.1
Bending tensile strength	[N mm ⁻²]	28 d	≥4.5 ^{c)}	5.4	0.1	3.9	0.1
Splitting tensile strength (lower cylindrical slices 50 mm height, 100 mm diameter) ^{d)}	[N mm ⁻²]	28 d	≥3.3 ^{d)}	4.4	0.2	3.7	0.3
Static elastic modulus	[GPa]	28 d	–	28.9	0.3	21.4	0.2

^{a)}Characteristic compressive strength (f_{ck,cube}); limit value referring to TL Beton-StB 07; ^{b)}Calculation referring to DIN EN 12 390-3^[139] Anhang NA for dry storage at 20 °C, 65% RH; f_{c,cube} = 0.92 × f_{c,dry}; ^{c)}Limit value referring to TL Beton-StB 07; ^{d)}Test method and limit value referring to FGSV AL Sp-Beton – 2016 Blatt 1.

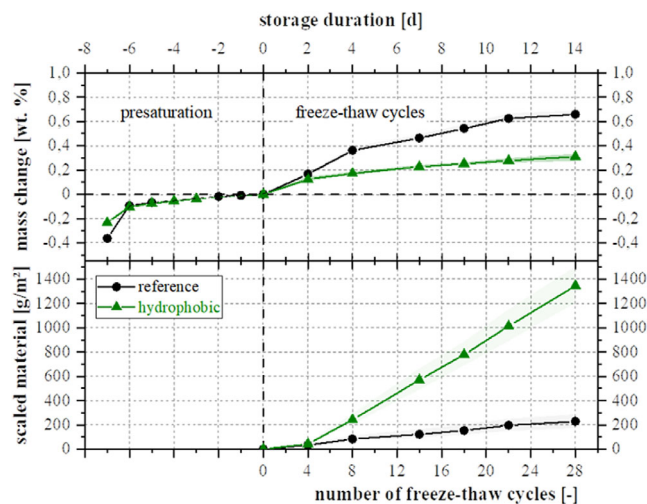


Figure 36. Comparison of resistance to freeze-thaw with deicing salt with-out and with HA. Above: bulk moisture change measured by mass change during presaturation phase and CDF test. Below: Surface scaling during CDF test.

strength properties are sufficient to obtain a concrete mix with the addition of hydrophobing agent that meets all requirements.

In addition to the mechanical properties, the addition of the HA also deteriorates the freeze-thaw resistance of the exposed aggregate concrete. **Figure 36** shows the amount of absorbed testing solution and of scaled material, respectively, during the CDF test.

Despite the fact that internal hydrophobic concrete absorbs much less testing solution during the presaturation phase and freeze-thaw cycle phase, it shows a significant increase in the amount of scaled material. A complicating factor in determining the cause of this behavior is that the freeze-thaw resistance of concrete is influenced by many parameters. It can be assumed that, probably among others, critical moisture saturation,^[143] the structure of meso- and macropores, air void distribution, strength properties, and curing conditions^[144,145] are the crucial factors negatively influencing the resistance of internal hydrophobic concrete to freeze-thaw with deicing salt. Elucidating the significance of these influencing factors is subject of current investigations.

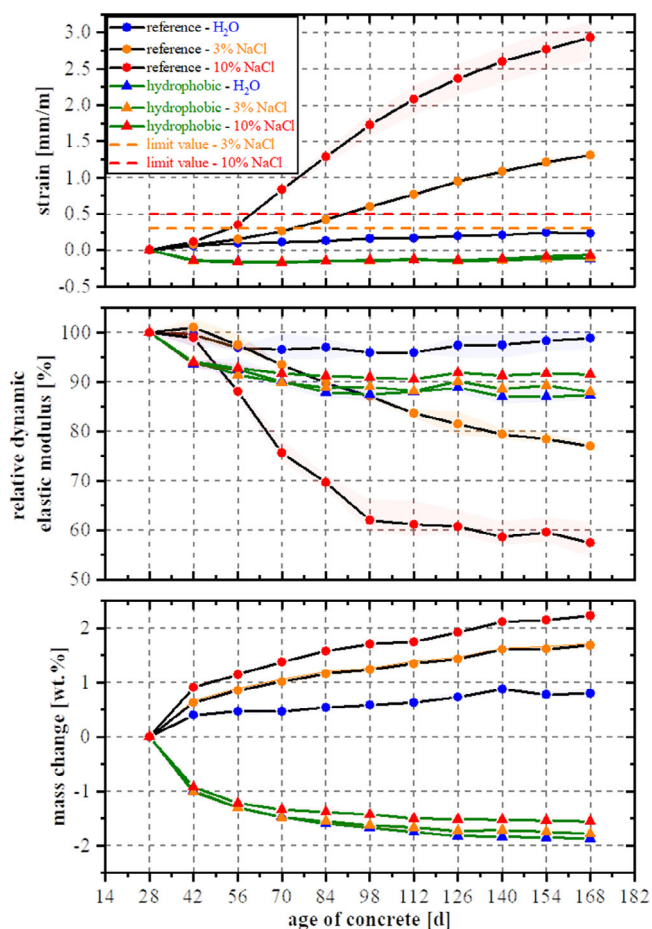


Figure 37. Strain, relative dynamic elastic modulus, and mass change during 60 °C concrete prism test with alkali supply without and with HA. No external alkali supply in concrete prisms immersed into H₂O.

5.4.3. Influence of HAs on Damaging ASR

The effect of the hydrophobizing agent on damaging ASR was verified with the two ASR concrete tests with alkali supply described in Section 3.8. Here, in addition to strain and mass, the usual condition and damage indicators, the relative dynamic elastic modulus was determined cyclically for better tracking of internal structural changes. This was realized by measuring the natural frequencies after excitation of a bending vibration.^[138] Furthermore, in the first test discussed below, the 60 °C concrete test with alkali supply, demineralized water was additionally used as a test medium to demonstrate the influence of deicing salt more clearly.

Figure 37 shows the findings of the 60 °C concrete prism test with alkali supply for exposed aggregate concrete without and with HA, giving the comparative values for expansion, relative dynamic elastic modulus, and mass in relation to concrete age. As expected, expansion increases in the reference concrete as the NaCl concentration of the deicing salt solution increases. The small increase in expansion when demineralized water is used is due to the fact that swelling processes primarily occur in the hardened cement paste. Because the aggregate used is

extremely alkali sensitive, when a 3% or 10% NaCl solution is applied, the expansion limit values are already exceeded after three or two cycles and by a multiple factor after ten cycles. This damage evolution is also reflected in the marked decrease in relative dynamic elastic modulus and the increased mass gain in the sample. In contrast, when HA is added, expansion of the sample is massively reduced below the limit value in each case when the three test liquids are applied. The negative expansion values that emerge throughout the entire course of the 60 °C concrete prism test with alkali supply with simultaneous mass reduction suggest that this is due to shrinkage processes. This implies that hydrophobized concrete absorbs moisture less efficiently in the immersion and fog phases of the individual cycles and releases moisture more efficiently in the drying phase. Because the test solution does not penetrate, this also means that conditions for ASR are not present. Therefore, the relative dynamic elastic modulus is almost unchanged from the first cycle on. This statement is supported by microscope investigations.^[129]

Comparable to the 60 °C concrete prism test with alkali supply, **Figure 38** shows the findings for the cyclic climate storage test of exposed aggregate concrete without and with HA, giving the comparative values for expansion, relative dynamic elastic modulus, and mass throughout storage duration or number of cycles. Because the aggregate used is extremely alkali sensitive, in this case, too, the reference concrete samples to which the different

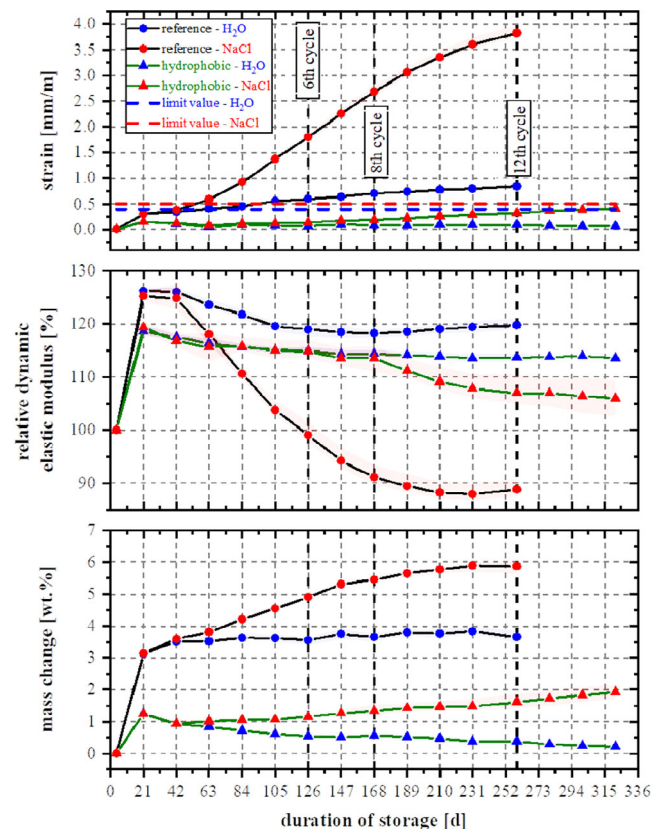


Figure 38. Strain, relative dynamic elastic modulus, and mass change during cyclic climate storage test without and with HA. No external alkali supply in concrete prisms applied with H₂O.

solutions were applied already exceed the expansion limit values after two cycles and by eight times (NaCl solution) or two times (demineralized water) after 12 cycles. The significantly higher damage evolution in the samples treated with NaCl solution is also reflected in a very marked reduction in relative dynamic elastic modulus and significantly greater increase in mass gain from the first cycle on. In this context, we note that the increase in relative dynamic elastic modulus and mass in the first cycle are the result of the sample's moisture absorption because the initial measurement takes place after the drying phase. This effect also occurs in reduced form in the hydrophobized exposed aggregate concrete during the first cycle.

Generally, applying HA to exposed aggregate concrete in cyclic climate storage tests with both test solutions results in a significant reduction in expansion far below the relevant limit value. It should be noted that the expansion of hydrophobized exposed aggregate concrete in cyclic climate storage tests when demineralized water was applied remains almost unchanged over 12 cycles. The moderate reduction also seen in relative dynamic elastic modulus and mass suggest that cyclic climate storage does not damage the internal structure. In contrast, when NaCl solution was applied to hydrophobized exposed aggregate concrete, a moderate increase in expansion occurred in the test specimens from the fifth cycle on. In this context, it is striking that this is accompanied by moderate mass gain on the one hand, and on the other, with increased reduction in relative dynamic elastic modulus from the eighth cycle onward. This suggests that under this level of stress, damage occurs to the internal structure. This finding is also confirmed by the thin section microscopic examinations that took place after the cyclic climate storage test.

Microscopic analysis showed that from the test specimen surface where NaCl solution was applied the damage gradient reached a maximum depth of 35 mm in the specimen.^[130] This depth correlates with the deicing salt ingress determined by LIBS. The damage in the concrete boundary zone typically takes the form of cracks and only isolated occurrence of ASR features. This suggests that this type of damage is not caused by ASR alone, but that other overlying damage mechanisms also contribute to it. In future, expansion of the test specimens will be measured at different depths below the surface treated with test solution to determine damage gradients during cyclic climate storage. Finally, it should be noted that in the hydrophobized exposed aggregate concrete examined here, the expansion limit value of test specimens to which NaCl solution was applied was not exceeded even after three additional cycles.

Conclusion and Outlook: The findings of the tests to assess the performance of internal hydrophobization as a novel ASR avoidance strategy for concrete road pavement using an exposed aggregate concrete formula with a very alkali-sensitive graywacke and the silane/siloxane-based HA used here^[137] permit the following conclusions: 1) Need for a higher dosage of air entrainment agent when using HA in fresh concrete to ensure the air void parameters required by the standards and adequate workability. 2) Deterioration of mechanical properties and of frost–deicing salt resistance in hydrophobized exposed aggregate concrete. 3) Proof that internal hydrophobization results in significant reduction of moisture and deicing salt penetration and the resulting ASR damage. a) More critical evaluation of the ASR damage process in hydrophobized exposed aggregate concrete in cyclic

climatic storage tests than in the 60 °C concrete prism test with alkali supply (increased expansion, more deicing salt input, emergence of a damage gradient, isolated ASR features in concrete boundary zone in which NaCl solution penetrated to a depth of up to approximately 35 mm). b) Improved registration of internal structural changes in pavement concrete in ASR concrete tests with alkali supply by: i) Additional cyclic determination of relative dynamic elastic modulus by measuring natural frequency. ii) Depth-related resolution of expansion of hydrophobized pavement concrete to better reflects the damage gradient in the sample during cyclic climate storage test. Preliminary results show plausible evidence of damage gradient by divergence of the strain values measured at different depths in the test specimen

To sum up, it can be stated that internal hydrophobization certainly has the potential to enable borderline alkali-sensitive aggregates to be used in concrete pavement. The conditions for this are, on the one hand, that the deterioration in mechanical properties and frost–deicing salt resistance must be minimized and, on the other hand, that the robustness of the mixture must be ensured in practice during construction. The thorough tests necessary for this are currently being carried out in a follow-up research project that is also funded by the BAST. It should be noted that initial findings where the dose of HA in exposed aggregate concrete is halved (from 2.0 M% to 1.0 M% in relation to cement content) are promising because they enable a significant improvement of mechanical properties and of frost–deicing salt resistance while the ASR performance is still adequate.

6. Conclusion and Outlook

Great efforts are being made worldwide to reduce the considerable economic impact caused by ASR damage to concrete structures and pavements. The overall aim of the review was to illustrate the interdisciplinary and cross scale research approach at BAM based on selected examples of recent and current work and to put it in the international context. Presenting specific aspects of the research for the first time in such breadth indicates the holistic approach necessary to tackle the problem.

After a general introduction to the problem including Germany's unique approach of preclassifying aggregates, a variety of methods for the verification and characterization of the damage mechanism and associated phenomena are presented. The methodology ranges from the visualization of cracks using 3D-CT, to the analysis of moisture and salt profiles by radar, NMR, and LIBS measurements, to the identification and characterization of reaction products with the help of optical microscopy, Raman spectra, and element distribution images acquired by micro-XRF.

In the third section, the general methodology for the assessment of ASR risk in new and existing structures is explained and the corresponding test methods specified by RILEM and American and German standards are listed by way of example. Based on the current state of knowledge, an accelerated concrete prism test developed by BAM is presented which prevents measurement artifacts by allowing continuous damage analysis in high resolution. Finally, the German methodology for preventing ASR damage in the construction of new concrete pavements is

explained as this is essential to understand the following case studies.

Serious deterioration due to ASR only becomes visible when the expansion reactions and resulting crack formation on the nano- and micro-levels accumulate to result in deformations on the meso- and macro-levels. Investigation of these microstructural mechanisms is therefore fundamental to interpreting the damage mechanism if ASR is involved. Section 4 uses two examples to illustrate how ASR can be verified as the cause of damage and differentiated from ettringite formation, by combining 3D-CT of drill cores with further analysis of the aggregate grain by microscopy and micro-XRF. Despite years of research, it has not yet been possible to elucidate in detail the microstructure of the damage products containing nano- and microcrystalline as well as amorphous components as a function of concrete formulation, exposure conditions, and mechanical loads, and to derive quantitative relationships to the expansion behavior of the reaction products. The results of a feasibility study presented in Section 4 illustrate that ASRP can be spatially differentiated by their Raman spectra. With progressive crack length through the cementitious matrix, the chemical structure and composition of the reaction product change due to the incorporation of calcium. The boundary conditions of the test procedures also seem to be reflected in the reaction products and the corresponding spectra.

Section 5 focuses on concrete pavements, due to the increased occurrence of ASR damage on the sections of the German highway network built before 2006. First, a comprehensive testing methodology for existing concrete pavements is presented. It consists of visual inspection and selection of sampling points, subsequent visual and microscopic investigation of the core samples, and determination of the deicing salt penetration using LIBS. In the last step, the residual damage potential is identified by application of a specific concrete test. For the validity of the visual inspection, the relation between the darkening of the pavement surface near the joints and increased moisture penetration into the concrete could be proven beyond doubt by combining two nondestructive measurements: radar and NMR. Regarding the analysis of the deicing salt penetration using LIBS, measurements of core samples are presented which show a good qualitative correlation of the sodium and chloride profiles with the results of wet chemistry and have the advantage of a higher depth resolution. The suspected cause for the higher sodium content determined by wet chemical analysis is topic of further research. The section ends with the presentation of promising research into a novel strategy to avoid ASR based on adding hydrophobing agents to the concrete mixture. If the deterioration in mechanical properties and frost–deicing salt resistance can be further minimized and at the same time the robustness of the mixture enhanced, borderline alkali-sensitive aggregates could be used in the mix design.

The variety of methods presented for assessing the risk of damage due to ASR for new constructions or analyzing the severity of damage that has already occurred illustrate that new insights into the damage mechanisms can be gained by using different starting points. On the one hand, visually detectable macroscopic damage like darkening of the concrete surface or crack formation can be used for digging deeper into the problem. In contrast, starting with basic research aims first at identifying

the underlying processes on the nano- and micro-level and from there tries to derive the subsequent consequences on the macro-level. At BAM both approaches are used simultaneously to deepen the understanding of ASR damage to concrete and to improve the testing methodology for risks assessment.

Also, BAM's current research activities focus on very different scales. Internal hydrophobization as a novel AKR avoidance strategy is further optimized and is to be tested in practice for the first time. In a second project, ASRP are now systematically analyzed by Raman spectroscopy, complemented by SEM/EDX as well as micro-XRF, to investigate the impact of different ASR provoking storage conditions on the chemical composition and structure of the reaction products formed in a variety of model concretes in temporal and local resolution. These findings are then compared to the data collected from ASR products in deteriorated structures. If the structure of the ASR products, depending on their genesis, can be fully elucidated in further research in and outside BAM, the testing methodology could one day be based on a scientific rather than a phenomenological approach.

It is further planned to use the automatic benchtop reactor—developed for the simultaneous detection of internal structural change within the 60 °C accelerated concrete prism test—to systematically analyze the kinetics of the ASR damage process for different types of concretes. Furthermore, based on their preliminary investigations, the influence of concrete degradation induced by cyclic compressive loading on harmful ASR in concrete pavement should be investigated in a realistic context, taking the interaction of moisture and deicing salt input into consideration.^[125] Of course, the results of all BAM research activities will be reflected within national and international committee work.

Looking further, it is important to put the ASR problem into the context of two important megatrends of our time: first, the aim of enhancing the sustainability of concrete by replacing Portland cement^[146,147] and by recycling aggregates instead of mining them. Many alternatives to established supplementary cementitious materials are currently being researched and the first binders based on alkali-activated materials (AAMs), limestone calcined clay and cement (LC3), and locally available alternative binders manufactured from residues are already on the market.^[148–151]

Changes in the concrete mixture must be carefully evaluated to establish whether existing standards for assessing aggregate reactivity toward AER need to be adapted. This applies specifically to the German Alkali Guideline where the accelerated tests are based on a Portland cement mixture and therefore can complicate the use of unconventional solutions.^[152,153] The second megatrend affecting the damage mechanism of ASR is ongoing climate change. The general rise in average temperature and in precipitation in the winter months^[154] anticipated for Germany suggests that the problem will worsen. Specific research on the impact of rapidly changing climate conditions on the formation of ASR is already in progress.^[155]

BAM is already active in a RILEM TC which initiated a round robin test for assessing sulfate resistance, ASR, and freeze-thaw resistance of alkali-activated concretes,^[156] and will continue to transfer the knowledge gained through its many years of research on ASR to the materials and boundary conditions of the future.

Acknowledgements

The authors would like to thank Dr.-Ing. Ludwig Stelzner, Philipp Drabetzki, Daniel Werner, Wilma Wallau, Sandra Sigmund, Dr.-Ing. Enno Krütt, Gerd Wilsch, Dr. Thomas Kind, and Jens Wöstmann for conducting experiments and analyzing research results and Bridget Schäfer for the proofreading. Furthermore, the authors would like to express their thank to the Federal Ministry of Transport and Digital Infrastructure, represented by the Federal Highway Research Institute (BAST), for the many years of active cooperation.

Open Access funding enabled and organized by Projekt DEAL.

Conflict of Interest

The authors declare no conflict of interest.

Keywords

accelerated testing, alkali-silica reaction, concrete, damage analysis, microstructure, mitigation strategies, nondestructive testing, road pavements

Received: September 30, 2021

Revised: April 14, 2022

Published online:

- [1] P. K. Mehta, P. J. M. Monteiro, *Concrete: Microstructure, Properties, and Materials*, McGraw-Hill, New York **2006**.
- [2] A. M. Neville, J. J. Brooks, *Concrete Technology*, Prentice Hall, Harlow **2010**.
- [3] H. F. W. Taylor, *Cement Chemistry*, Academic Press, London **1990**.
- [4] P. C. Hewlett, M. Liska, *Lea's Chemistry of Cement and Concrete*, Butterworth-Heinemann, Oxford, UK **2019**.
- [5] Ed. Mindess, *Developments in the Formulation And Reinforcement of Concrete*, Elsevier, Woodhead Publishing, Kidlington, MA **2019**.
- [6] C. L. Page, M. M. Page, *Durability of Concrete and Cement Composites*, CRC Press, Boca Raton, FL **2007**.
- [7] G. E. Blight, M. G. Alexander, *Alkali-Aggregate Reaction and Structural Damage to Concrete: Engineering Assessment, Repair And Management*, CRC Press, Boca Raton, FL **2011**.
- [8] P. J. Nixon, I. Sims, *RILEM Recommendations for The Prevention of Damage by Alkali-Aggregate Reactions in New Concrete Structures: State-of-The-Art Report of the RILEM Technical Committee 219-ACS*, Springer, Dordrecht **2016**.
- [9] R. N. Swamy, *Alkali-Silica Reaction in Concrete*, CRC Press, London **1991**.
- [10] R. B. Figueira, R. Sousa, L. Coelho, M. Azenha, J. M. de Almeida, P. A. S. Jorge, C. J. R. Silva, *Construct. Build. Mater.* **2019**, 222, 903.
- [11] M. Barreto Santos, J. De Brito, A. Santos Silva, *Materials* **2020**, 13, 2625.
- [12] G. Geng, S. Barbotin, M. Shakoorkoskooie, Z. Shi, A. Leemann, D. F. Sanchez, D. Grolimund, E. Wieland, R. Dähn, *Cement Concrete Res.* **2021**, 141, 106331.
- [13] K. Peterson, D. Gress, T. Van Dam, L. Sutter, *Cement Concrete Res.* **2006**, 36, 1523.
- [14] Y. Ando, T. Katayama, S. Hirono, T. Sato, T. Noguchi, in *Cases of Deterioration*, ICAAR, Sao Paulo, Brazil **2016**, p. 10.
- [15] W. Wedekind, A. Protz, in *Geophysical Research Abstracts*, 18, Copernicus Publications, Vienna Austria **2016**, p. 1.
- [16] B. Fournier, M.-A. Bérubé, *Can. J. Civ. Eng.* **2000**, 27, 167.
- [17] M. Thomas, *Cement Concrete Res.* **2011**, 41, 1224.
- [18] J. Lindgård, Ö. Andiç-Çakır, I. Fernandes, T. F. Rønning, M. D. A. Thomas, *Cement Concrete Res.* **2012**, 42, 223.
- [19] B. Godart, M. de Rooij, J. G. M. Wood, *Guide to Diagnosis and Appraisal of AAR Damage to Concrete in Structures*, Springer, Dordrecht **2013**.
- [20] V. Saouma, *Diagnosis & Prognosis of AAR Affected Structures: State-of-the-Art Report of The RILEM Technical Committee 259-ISR*, Springer International Publishing, Cham **2021**.
- [21] W. Li, Z. Huang, F. Cao, Z. Sun, S. P. Shah, *Construct. Build. Mater.* **2015**, 95, 366.
- [22] J. Lindgård, E. J. Sellevold, M. D. A. Thomas, B. Pedersen, H. Justnes, T. F. Rønning, *Cement Concrete Res.* **2013**, 53, 145.
- [23] T. E. Stanton, *T. Am. Soc. Civ. Eng.* **1942**, 107, 54.
- [24] H. de Mayo Bernardes, N. Hasparyk-Pagan, *Proc. of the 15 Int. Conf. on Alkali-Aggregate Reaction in Concrete*, ICAAR, Sao Paulo, Brazil **2016**.
- [25] I. Fernandes, M. dos A. Ribeiro, H. Martins, M. Broekmans, I. Sims, P. Nixon, F. Noronha, in *Engineering Geology for Society and Territory*, Vol. 5 (Eds: G. Lollino, A. Manconi, F. Guzzetti, M. Culshaw, P. Bobrowsky, F. Luino), Springer International Publishing, Cham **2015**, p. 37.
- [26] I. Sims, P. Nixon, *Mat. Struct.* **2003**, 36, 480.
- [27] I. Sims, P. J. Nixon, *Rilem Recommendations for The Prevention of Damage by Alkali-Aggregate in New Concrete Structures - State-of-the-Art Report of The RILEM Technical Committee 219-ACS*, Springer, Dordrecht, Netherlands **2016**.
- [28] I. Borchers, J. Lindgård, T. F. Rønning, B. J. Wigum, *Mater. Struct.* **2021**, 54, 203.
- [29] I. Borchers, *Mater. Struct.* **2021**, 54, 202.
- [30] Rønning et al., in *Proc. of the 16th Int. Conf. on Alkali-Aggregate Reaction in Concrete*, 1, LNEC, Lisbon **2021**, p. 815.
- [31] I. Fernandes, M. dos A. Ribeiro, M. A. T. M. Broekmans, I. Sims, *RILEM AAR 1.2: Petrographic Atlas: Characterisation of Aggregates Regarding Potential Reactivity to Alkalis: RILEM TC 219-ACS Recommended Guidance AAR-1.2, for Use with the RILEM AAR-1.1 Petrographic Examination Method*, Springer, New York **2016**.
- [32] R. Hooton, C. Rogers, T. Ramlochan, *MJ* **2013**, 110, 539.
- [33] J. Tanesi, T. Drimalas, K. S. T. Chopperla, M. Beyene, J. H. Ideker, H. Kim, L. Montanari, A. Ardani, *Transport. Res. Record* **2020**, 2674, 120.
- [34] J. Lindgård, P. J. Nixon, I. Borchers, B. Schouenborg, B. J. Wigum, M. Haugen, U. Åkesson, *Cement Concrete Res.* **2010**, 40, 611.
- [35] A. Abd-elssamd, S. Le Pape, Z. John Ma, Y. le Pape, S. Johnson, in *Diagnosis & Prognosis of AAR Affected Structures* (Ed: V. E. Saouma), Springer International Publishing, Cham **2021**, p. 247.
- [36] S. Matthews, *Struct. Conc.* **2017**, 18, 651.
- [37] G. Davies, R. E. Oberholster, *An Interlaboratory Test Programme on the NBRI Accelerated Test to Determine the Alkali-Reactivity of Aggregates*, National Building Research Institute, Pretoria, South Africa **1987**.
- [38] ASTM, *Standard Test Method for Potential Alkali Reactivity of Aggregates (Mortar-Bar Method)*, ASTM C1260-01, ASTM International, West Conshohocken, PA **2001**.
- [39] ASTM, *Standard Test Method for Determination of Length Change of Concrete Due to Alkali-Silica Reaction*, ASTM C1293 - 20a, ASTM International, West Conshohocken, PA **2020**.
- [40] S. Beauchemin, B. Fournier, J. Duchesne, *Cement Concrete Res.* **2018**, 104, 25.
- [41] DAfStb, *Vorbeugende Maßnahmen gegen schädigende Alkalireaktion im Beton (Alkali-Richtlinie)*, Deutschen Ausschuss für Stahlbeton, Berlin, Germany **2013**.
- [42] DIN, *Aggregates for concrete; German version EN 12620:2002+A1:2008*, DIN EN 12620, German Institute for Standardization, Berlin, Germany **2008**.

- [43] DIN, *Concrete, Reinforced and Prestressed Concrete Structures – Part 2: Concrete – Specification, Properties, Production and Conformity – Application Rules for DIN EN 206-1; DIN 1045-2*, German Institute for Standardization, Berlin, Germany **2008**.
- [44] C. Öttl, *Die schädigende Alkalireaktion von gebrochener Oberrhein-Gesteinskörnung im Beton*, Otto-Graf-Institut, Stuttgart **2004**.
- [45] J. Stark, E. Freyburg, K. Seyfarth, C. Giebson, D. Erfurt, *ZKG Int.* **2010**, 86.
- [46] ARS, *Prevention of Damage to Concrete Pavements as a Result of Alkali-Silica Reaction; General Circular for Road Construction (ARS) 12/2006*, Federal Ministry of Transport, Building and Urban Development, Bonn, Germany **2006**.
- [47] ARS, *Prevention of Damage to Concrete Pavements as a Result of Alkali-Silica Reaction; General Circular for Road Construction (ARS) 04/2013*, Federal Ministry of Transport, Building and Urban Development, Bonn, Germany **2013**.
- [48] C. F. Ferraris, *Alkali-Silica Reaction and High Performance Concrete*, National Institute of Standards And Technology, Gaithersburg, MD **1995**.
- [49] M. A. T. M. Broekmans, *Mater. Character.* **2004**, 53, 129.
- [50] D. Werner, A. Gardei, S. Simon, B. Meng, in *Proc. of the 15th Euroseminar on Microscopy Applied to Building Materials (15th EMABM)*, Delft University of Technology, Delft, The Netherlands **2015**, p. 10.
- [51] K. Voland, *Einfluss der Porosität von Beton auf den Ablauf einer schädigenden Alkali-Kieselsäure-Reaktion*, Bundesanstalt für Materialforschung und -prüfung (BAM), Berlin **2016**.
- [52] A. Gholizadeh-Vayghan, F. Rajabipour, *Cement Concrete Res.* **2017**, 94, 49.
- [53] N. Thaulow, U. H. Jakobsen, B. Clark, *Cement Concrete Res.* **1996**, 26, 309.
- [54] T. Knudsen, N. Thaulow, *Cement Concrete Res.* **1975**, 5, 443.
- [55] H. Aguiar, J. Serra, P. González, B. León, *J. Non-Cryst. Solids* **2009**, 355, 475.
- [56] S. P. Rossano, B. Mysen, in *Raman Spectroscopy Applied to Earth Sciences and Cultural Heritage* (Eds: G. Ferraris, J. Dubessy, M.-C. Caumon, F. Rull), European Mineralogical Union, Twickenham, UK **2012**, pp. 321–366, ISBN 978-0-903056-31-1, <https://doi.org/10.1180/EMU-notes.12.9>.
- [57] G. Geng, Z. Shi, A. Leemann, C. Borca, T. Huthwelker, K. Glazyrin, I. V. Pekov, S. Churakov, B. Lothenbach, R. Dähn, E. Wieland, *Cement Concrete Res.* **2020**, 129, 105958.
- [58] X. Hou, R. J. Kirkpatrick, L. J. Struble, P. J. M. Monteiro, *J. Am. Ceram. Soc.* **2005**, 88, 7.
- [59] A. Leemann, Z. Shi, J. Lindgård, *Cement Concrete Res.* **2020**, 137, 106190.
- [60] E. Boehm-Courjault, S. Barbotin, A. Leemann, K. Scrivener, *Cement Concrete Res.* **2020**, 130, 105988.
- [61] R. Dähn, A. Arakcheeva, P. Schaub, P. Pattison, G. Chapuis, D. Grolimund, E. Wieland, A. Leemann, *Cement Concrete Res.* **2016**, 79, 49.
- [62] I. Fernandes, *Mater. Character.* **2009**, 60, 655.
- [63] M. Wojdyr, *J. Appl. Cryst.* **2010**, 43, 3.
- [64] P. Hahn-Weinheimer, A. Hirner, K. Weber-Diefenbach, *Röntgenfluoreszenzanalytische Methoden - Grundlagen Und Praktische Anwendung In Den Geo-, Material- Und Umweltwissenschaften*, Springer, Berlin, Germany **2000**.
- [65] G. West, *Alkali-Aggregate Reaction in Concrete Roads and Bridges*, Thomas Telford Publishing, London **1996**.
- [66] H. Wiggenhauser, D. Schaurich, G. Wilsch, *NDT & E Int.* **1998**, 31, 307.
- [67] G. Wilsch, F. Weritz, D. Schaurich, H. Wiggenhauser, *Construct. Build. Mater.* **2005**, 19, 724.
- [68] F. Weritz, D. Schaurich, G. Wilsch, *Spectrochim. Acta Part B: Atomic Spectrosc.* **2007**, 62, 1504.
- [69] S. Millar, G. Wilsch, T. Eichler, C. Gottlieb, H. Wiggenhauser, *Beton- und Stahlbetonbau* **2015**, 110, 501.
- [70] A. Taffe, G. Wilsch, D. Schaurich, F. Weritz, *Beton- Stahlbetonbau* **2008**, 103, 14.
- [71] A. Taffe, G. Wilsch, D. Schaurich, F. Weritz, *Beton- Stahlbetonbau* **2008**, 103, 16.
- [72] German Society for Non-Destructive Testing, *Leaflet on the Radar Method for Non-Destructive Testing in the Construction Industry*, **2008**.
- [73] D. Lu, X. Zhou, Z. Xu, X. Lan, M. Tang, B. Fournier, *Cement Concrete Res.* **2006**, 36, 1157.
- [74] M. A. Bérubé, J. F. Dorion, J. Duchesne, B. Fournier, D. Vézina, *Cement Concrete Res.* **2003**, 33, 77.
- [75] ASTM, *Standard Test Method for Potential Alkali-Silica Reactivity of Aggregates (Chemical Method)*, ASTM C289-07, ASTM International, West Conshohocken, PA **2007**.
- [76] J. E. Gillott, *Eng. Geol.* **1975**, 9, 303.
- [77] T. Ichikawa, *Cement Concrete Res.* **2009**, 39, 716.
- [78] D. Constantiner, S. Diamond, *Cement Concrete Res.* **2003**, 33, 549.
- [79] E. Menéndez, A. S. Silva, J. Duchesne, *Mater. Struct.* **2021**, 54, 205.
- [80] F. Weise, S. Millar, G. Wilsch, *Beton- Stahlbetonbau* **2018**, 113, 656.
- [81] W. Wallau, S. Pirsawetz, K. Voland, B. Meng, *Mater. Struct.* **2018**, 51, 79.
- [82] F. Weise, S. Pirsawetz, B. Maier, K. Voland, *Kontinuierliche Dehnungsmessung bei Prüfung des Einflusses der Alkali-Kieselsäure-Reaktion auf Gefügeveränderungen in Betonen*, **2011**, EP 2397848 A1.
- [83] C. Müller, F. Weise, I. Borchers, K. Voland, Federal Ministry For Economic Affairs And Energy (BMWi), Berlin, Germany **2010**.
- [84] F. Weise, K. Voland, S. Pirsawetz, D. Meinel, in (Eds: T. Drimalas, J.H. Ideker, B. Fournier), in *Proceedings of the 14th International Conference on Alkali Aggregate Reaction (ICAAR)*, FARIN (Forum for Alkali Reaction In Norway), Austin, TX, USA, May 20–25 **2012**, no. 021811-WEIS, pp. 20–25.
- [85] F. Weise, K. Voland, S. Pirsawetz, D. Meinel, *Beton- Stahlbetonbau* **2012**, 107, 805.
- [86] W. Wallau, S. Pirsawetz, M. Greim, O. Teubert, Bundesanstalt für Materialforschung und -prüfung, S.G.T. u G. GmbH, AKR-Schadensmonitoring Im 60°C-Betonversuch: Abschlussbericht zum MNPQ-Projekt (19/14): Bearbeitungszeitraum: September 2015 - August 2017, Bundesanstalt für Materialforschung und -Prüfung, Berlin, Germany **2017**.
- [87] E. Krütt, W. Wallau, B. Meng, M. Greim, S. Pirsawetz, *Beton- Stahlbetonbau* **2019**, 114, 911.
- [88] Nixon & Sims, in *RILEM State Art Reports*, Vol. 17, Springer, Dordrecht **2015**, <https://doi.org/10.1007/978-94-017-7252-5>, ISBN 978-94-017-7251-8.
- [89] FGSV, *Richtlinien Für Die Standardisierung Des Oberbaus Von Verkehrsflächen, RStO 12* Forschungsgesellschaft für Straßen- und Verkehrswesen, Köln **2012**.
- [90] FGSV, *Technische Prüfvorschriften Für Verkehrsflächenbefestigungen - Betonbauweisen, TP B-StB*, Forschungsgesellschaft für Straßen- und Verkehrswesen, Köln **2021**.
- [91] C. Müller, I. Borchers, E. Eickschen, *BUST* **2007**, 102, 528.
- [92] K. Seyfarth, K. Dombrowski, in *4. Baustoffkolloquium TU Bergakademie Freiberg, Professur Bergbau – Tagebau, Freiberg* **2004**, p. 78.
- [93] F. Weise, S. Pirsawetz, B. Meng, in *RILEM Symposium on On Site Assessment of Concrete, Masonry and Timber Structures*, RILEM Publications SARL, Varenna, Italy **2008**, p. 483.
- [94] O. R. Batic, C. A. Milanesi, P. J. Maiza, S. A. Marfil, *Cement Concrete Res.* **2000**, 30, 1407.

- [95] S. Bauer, *Alkali-Silica Reaction and Delayed Ettringite Formation in Concrete: A Literature Review*, Center for Transportation Research, Texas **2001**.
- [96] S. O. Okolu, M. D. A. Thomas, R. D. Hooton, *Cement Concrete Res.* **2007**, 37, 942.
- [97] Y. Kawabata, N. Ueda, T. Miura, S. Multon, *Cement Concrete Compos.* **2021**, 121, 104062.
- [98] A. Shayan, I. Ivanusec, *Cement Concrete Compos.* **1996**, 18, 161.
- [99] U. Müller, P. G. Bürgisser, F. Weise, B. Meng, in *Concrete Under Severe Conditions - Environment and Loading (CONSEC' 10)* Taylor & Francis, Mérida, México **2010**, p. 7.
- [100] S. Simon, S. Sigmund, M. A. Ziemann, in *Proc. of the 15th Int. Congress on the Chemistry of Cement*, Prague, Czech Republic **2019**, p. 11.
- [101] A. Leemann, *Cement Concrete Res.* **2017**, 102, 41.
- [102] T.-C. Ling, C. Balachandran, J. F. Muñoz, J. Youtcheff, *Mater. Struct.* **2018**, 51, 1.
- [103] A. Leemann, Z. Shi, M. Wyrzykowski, F. Winnefeld, *Mater. Des.* **2020**, 195, 109066.
- [104] Z. Shi, B. Lothenbach, *Cement Concrete Res.* **2020**, 127, 105914.
- [105] F. Rajabipour, E. Giannini, C. Dunant, J. H. Ideker, M. D. A. Thomas, *Cement Concrete Res.* **2015**, 76, 130.
- [106] T. Schmid, P. Dariz, *Heritage* **2019**, 2, 1662.
- [107] C. Balachandran, J. F. Muñoz, T. Arnold, *Cement Concrete Res.* **2017**, 92, 66.
- [108] Z. Shi, B. Lothenbach, *Cement Concrete Res.* **2019**, 126, 105898.
- [109] X. Hou, L. J. Struble, R. J. Kirkpatrick, *Cement Concrete Res.* **2004**, 34, 1683.
- [110] C. S. Walker, S. Sutou, C. Oda, M. Mihara, A. Honda, *Cement Concrete Res.* **2016**, 79, 1.
- [111] C. E. Tambelli, J. F. Schneider, N. P. Hasparyk, P. J. M. Monteiro, *J. Non-Cryst. Solids* **2006**, 352, p. 3429.
- [112] B. Lothenbach, A. Nonat, *Cement Concrete Res.* **2015**, 78, 57.
- [113] A. Leemann, C. Merz, *Cement Concrete Res.* **2013**, 49, 29.
- [114] Z. Shi, S. Park, B. Lothenbach, A. Leemann, *Cement Concrete Res.* **2020**, 137, 106213.
- [115] F. Weise, T. Kind, L. Stelzner, M. Wieland, *Beton- Stahlbetonbau* **2018**, 113, 647.
- [116] F. Weise, B. Maier, J. Kronemann, D. Werner, S. Millar, *AKR Preliminary Investigations on Drill Cores of Concrete Pavements*, Federal Ministry of Transport, Building and Urban Development (BMVBS), Berlin, Germany **2016**.
- [117] F. Weise, B. Maier, D. Werner, G. Wilsch, *Evaluation of ASR Testing Methods in Relation to Specific Damage Categories*, Federal Ministry of Transport and Digital Infrastructure (BMVI), Berlin, Germany **2021**.
- [118] C. Giebson, K. Voland, H.-M. Ludwig, B. Meng, *Beton-Stahlbetonbau* **2015**, 110, 13.
- [119] F. Weise, A. Wiedmann, K. Voland, E. Kotan, K. Ehrig, H. S. Müller, *Beton- Stahlbetonbau* **2015**, 110, 22.
- [120] R. Przondziona, J. Timothy, M. Nguyen, F. Weise, R. Breitenbücher, G. Meschke, B. Meng, *Beton- Stahlbetonbau* **2015**, 110, 3.
- [121] F. Weise, K. Voland, S. Pirsakawetz, B. Meng, in *Factors Affecting AAR*, ICAAR, Sao Paulo, Brazil **2016**, p. 11.
- [122] A. Wiedmann, F. Weise, E. Kotan, H. S. Müller, B. Meng, *Struct. Concrete* **2017**, 18, 539.
- [123] R. Przondziona, J. Timothy, F. Weise, E. Krütt, R. Breitenbücher, G. Meschke, M. Hofmann, *Struct. Concrete* **2017**, 18, 519.
- [124] F. Weise, E. Krütt, B. Meng, F.A. Finger-Institut Für Baustoffkunde, Bauhaus-Universität Weimar, Weimar, Germany **2018**, p. 13.
- [125] E. Krütt, F. Weise, B. Meng, *Beton- Stahlbetonbau* **2020**, 115, 779.
- [126] E. Krütt, *Untersuchungen Zur Auswirkung Einer Ermüdungsbedingten Betondegradation Im Fahrhanddeckenbeton Auf Die Schädigende Alkali-Kieselsäure-Reaktion*, Ruhr-Universität Bochum, Bochum **2020**.
- [127] F. Weise, M. Kositz, T. Oesch, K.-J. Hüniger, G. Wilsch, S. Sigmund, *Analysis of the Microstructure Depending Solubility Behavior of Potential ASR Sensitive Aggregates* Bundesanstalt für Straßenwesen (BASt), Berlin, Germany **2021**.
- [128] T. Oesch, F. Weise, H. Marx, M. Kositz, K.-J. Huenger, in *4th Int. Rilem Conf. on Microstructure Related Durability of Cementitious Composites*, Delft University of Technology - Southeast University, Den Haag, Netherlands **2021**.
- [129] F. Weise, M. Fladt, I. Meyer, *Bewertung Der Innenhydrophobierung Von Fahrhanddeckenbetonen Als Neuartige AKR-Vermeidungsstrategie*, Federal Ministry of Transport and Digital Infrastructure (BMVI), Berlin, Germany **2022**.
- [130] F. Weise, M. Fladt, M. Wieland, *Lisboa* **2021**, 511.
- [131] R. Angerer, *Empfehlungen für die Schadensdiagnose und die Bauliche Erhaltung von AKR-Geschädigten Fahrhanddecken aus Beton*, BASt, Bergisch Gladbach, Germany **2019**.
- [132] K. Seyfarth, C. Giebson, F. Weise, H.-M. Ludwig, R. Breitenbücher, *Futurum - Building Material Street Concrete*, Federal Ministry of Transport and Digital Infrastructure (BMVI), Weimar, Germany **2018**.
- [133] R. Springenschmid, H. Dorner, G. Kleiner, *Anleitung Zur Bestimmung Des Chloridgehaltes Von Beton*, Beuth, Berlin **1989**.
- [134] C. Gottlieb, S. Millar, T. Günther, G. Wilsch, *Spectrochim. Acta Part B: Atomic Spectrosc.* **2017**, 132, 43.
- [135] C. Gottlieb, T. Günther, G. Wilsch, *Spectrochim. Acta Part B: Atomic Spectros.* **2018**, 142, 74.
- [136] S. Millar, C. Gottlieb, T. Günther, N. Sankat, G. Wilsch, S. Kruschwitz, *Spectrochim. Acta Part B: Atomic Spectrosc.* **2018**, 147, 1.
- [137] D. Ballschuh, H. Seibt, A. Gerdes, J. Süßmuth, P. Schäffel, *Hydrophobierungsmittel für Mineralische Materialien*, **2020**, EP 3 725 753 A1.
- [138] DAFStb, *Prüfung von Beton-Empfehlungen und Hinweise als Ergänzung zu DIN 1048; Heft 422*, Deutschen Ausschuss Für Stahlbeton, Berlin, Germany **1991**.
- [139] DIN, *Testing Hardened Concrete - Part 3: Compressive Strength of Test Specimens; German Version EN 12390-3:2019*, German Institute for Standardization, Berlin, Germany **2019**.
- [140] DIN, *Testing Hardened Concrete - Part 5: Flexural Strength of Test Specimens; German Version EN 12390-5:2019*, German Institute for Standardization, Berlin, Germany **2019**.
- [141] DIN, *Testing Hardened Concrete - Part 13: Determination of Secant Modulus of Elasticity in Compression; German Version EN 12390-13:2021*, German Institute for Standardization, Berlin, Germany **2021**.
- [142] DIN, *Testing Hardened Concrete - Part 9: Freeze-Thaw Resistance with De-Icing Salts - Scaling; German Version CEN/TS 12390-9:2016*, German Institute for Standardization, Berlin, Germany **2017**.
- [143] G. Fagerlund, *Mat. Constr.* **1977**, 10, 231.
- [144] M. Haist, Z. Djuric, H. S. Müller, in *Dauerhafter Beton – Grundlagen, Planung und Ausführung bei Frost- und Frost-Taumittel-Beanspruchung*, Universitätsverlag Karlsruhe, Karlsruhe **2009**, p. 21.
- [145] U. Guse, in *Dauerhafter Beton – Grundlagen, Planung und Ausführung bei Frost- und Frost-Taumittel-Beanspruchung*, Universitätsverlag Karlsruhe, Karlsruhe **2009**, p. 43.
- [146] R. A. Data, *CISION PR Newswire* **2020**.
- [147] R. de Best, *Statista*, January 15 **2021**, <https://www.statista.com/statistics/587718/green-building-materials-market-outlook-worldwide/> (accessed: September 2021).
- [148] F. Bart, C. Cau-di-Coumes, F. Frizon, S. Lorente, in *Cement-Based Materials for Nuclear Waste Storage*, Springer, New York, NY **2013**.

- [149] L. Coppola, T. Bellezze, A. Belli, M. C. Bignozzi, F. Bolzoni, A. Brenna, M. Cabrini, S. Candamano, M. Cappai, D. Caputo, M. Carsana, L. Casnedi, R. Cioffi, O. Cocco, D. Coffetti, F. Colangelo, B. Coppola, V. Corinaldesi, F. Crea, E. Crotti, V. Daniele, S. D. Gisi, F. Delogu, M. V. Diamanti, L. D. Maio, R. D. Mundo, L. D. Palma, J. Donnini, I. Farina, C. Ferone, et al. *J. Appl. Biomater. Funct. Mater.* **2018**, *16*, 186.
- [150] M. C. G. Juenger, F. Winnefeld, J. L. Provis, J. H. Ideker, *Cement Concrete Res.* **2011**, *41*, 1232.
- [151] S. M. Levy, P. Helene, *Cement Concrete Res.* **2004**, *34*, 1975.
- [152] H.-P. Backes, D. Brandenburger, M. Meißner, *VGB PowerTech*, no. 12/2005, International Technical Association for the Generation and Storage of Electricity and Heat, Deilbachtal, Germany **2005**, <https://www.baumineral.de/downloads/file/77/ModernesBaustoffmanagementam-BeispielvonSFA.pdf> (accessed: May 2022).
- [153] R. Mellwitz, *SCHWENK News*, Ulm, Germany, February **2018**, <https://www.schwenk.de/recyclingbeton-baustoff-der-zukunft/> (accessed: May 2022).
- [154] D. Schröter, M. Zebisch, T. Grothmann, *Klimastatusbericht 2005*, Deutscher Wetterdienst, Offenbach, Germany **2006**, 44–56, https://www.dwd.de/DE/leistungen/klimastatusbericht/publikationen/ksb_2005.pdf?__blob=publicationFile&v=4 (accessed: May 2022).
- [155] J. H. Ideker, K. De Weerd, RILEM, D. Cluster, *Technical Committee 301-ASR, Activity Start*, Paris, France **2020**, <https://www.rilem.net/groupe/301-asr-risk-assessment-of-concrete-mixture-designs-with-alkali-silica-reactive-asr-aggregates-425> (accessed: May 2022).
- [156] F. Winnefeld, G. J. G. Gluth, S. A. Bernal, M. C. Bignozzi, L. Carabba, S. Chithiraputhiran, A. Dehghan, S. Dolenc, K. Dombrowski-Daube, A. Dubey, V. Ducman, Y. Jin, K. Peterson, D. Stephan, J. L. Provis, *Mater. Struct.* **2020**, *53*, 140.